

AD-A223 109

**Spectroscopy of Ions and Their Clusters**

**Terry A. Miller**

Ohio State University  
Research Foundation  
1314 Kinnear Road  
Columbus, OH 43212

1 December 1989

Final Report  
12 March 1986-30 November 1989

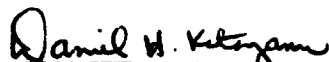
Approved for public release; distribution unlimited

GEOPHYSICS LABORATORY  
AIR FORCE SYSTEMS COMMAND  
UNITED STATES AIR FORCE  
HANSCOM AIR FORCE BASE, MASSACHUSETTS 01731-5000

DTIC  
ELECTE  
JUN 13 1990  
S B D  
CO

90 06 12 134

"This technical report has been reviewed and is approved for publication"



DANIEL H. KATAYAMA

Contract Manager

Ionospheric Modelling and  
Remote Sensing Branch



DAVID N. ANDERSON

Chief, Ionospheric Modelling and  
Remote Sensing Branch  
Ionospheric Physics Division

FOR THE COMMANDER



ROBERT A. SKRIVANEK

Division Director

This report has been reviewed by the ESD Public Affairs Office (PA) and is releasable to the National Technical Information Service (NTIS).

Qualified requestors may obtain additional copies from the Defense Technical Information Center. All others should apply to the National Technical Information Service.

If your address has changed, or if you wish to be removed from the mailing list, or if the addressee is no longer employed by your organization, please notify GL/IMA, Hanscom AFB, MA 01731. This will assist us in maintaining a current mailing list.

Do not return copies of this report unless contractual obligations or notices on a specific document requires that it be returned.

Unclassified

SECURITY CLASSIFICATION OF THIS PAGE

## REPORT DOCUMENTATION PAGE

1a. REPORT SECURITY CLASSIFICATION Unclassified			1b. RESTRICTIVE MARKINGS	
2a. SECURITY CLASSIFICATION AUTHORITY			3. DISTRIBUTION/AVAILABILITY OF REPORT Approved for public release; distribution unlimited.	
2b. DECLASSIFICATION/DOWNGRADING SCHEDULE				
4. PERFORMING ORGANIZATION REPORT NUMBER(S) 765285/718164			5. MONITORING ORGANIZATION REPORT NUMBER(S) GL-TR-89-0341	
6a. NAME OF PERFORMING ORGANIZATION The Ohio State University Research Foundation		6b. OFFICE SYMBOL (If applicable) OSURF	7a. NAME OF MONITORING ORGANIZATION Geophysics Laboratory	
6c. ADDRESS (City, State and ZIP Code) 1314 Kinnear Road Columbus, OH 43212			7b. ADDRESS (City, State and ZIP Code) Hanscom AFB Massachusetts 01731-5000	
8a. NAME OF FUNDING/SPONSORING ORGANIZATION		8b. OFFICE SYMBOL (If applicable)	9. PROCUREMENT INSTRUMENT IDENTIFICATION NUMBER F19628-86-K-0022	
8c. ADDRESS (City, State and ZIP Code)			10. SOURCE OF FUNDING NOS.	
			PROGRAM ELEMENT NO.	PROJECT NO.
			61102F	2303
			TASK NO.	WORK UNIT NO.
			G1	AI
11. TITLE (Include Security Classification) Spectroscopy of Ions and their Clusters (unclassified)				
12. PERSONAL AUTHOR(S) Terry A. Miller				
13a. TYPE OF REPORT Final		13b. TIME COVERED FROM 3/12/86 TO 11/30/89		14. DATE OF REPORT (Yr. Mo., Day) 1989/12/1
15. PAGE COUNT 64				
16. SUPPLEMENTARY NOTATION				
17. COSATI CODES			18. SUBJECT TERMS (Continue on reverse if necessary and identify by block number)	
FIELD	GROUP	SUB GR	Laser induced fluorescence, molecular ions, Atomic and Molecular Chemistry, clusters, complexed systems, etc.	
19. ABSTRACT (Continue on reverse if necessary and identify by block number)				
<p>Based upon mass spectrometric evidence as well as indirect speculations, molecular ions and their clusters have long been recognized as playing important roles in the chemistry of the earth's atmosphere. However, the (non-mass) spectroscopy of all large ions is difficult, with the spectroscopy of cluster ions being essentially non-existent.</p> <p>We are constructing a unique apparatus for the spectroscopic study of large ions, particularly ionic clusters. This apparatus allows the combination of laser induced fluorescence characterization of ions and their clusters while simultaneously identifying them by their time-of-flight mass spectra. This apparatus can make exciting contributions to our knowledge of how the electronic spectra of ions change as neutral species are clustered about them. Similarly, the manner in which such clusters react to radiation, i.e. fragmentation, fluorescence, etc., can be detailed by such experiments.</p>				
20. DISTRIBUTION/AVAILABILITY OF ABSTRACT UNCLASSIFIED/UNLIMITED <input checked="" type="checkbox"/> SAME AS RPT <input type="checkbox"/> DTIC USERS <input type="checkbox"/>			21. ABSTRACT SECURITY CLASSIFICATION Unclassified	
22a. NAME OF RESPONSIBLE INDIVIDUAL Daniel Katayama			22b. TELEPHONE NUMBER (Include Area Code) (617) 377-4042	22c. OFFICE SYMBOL GL/LIU

## I. INTRODUCTION

The study of clusters is a very active area in chemical physics today. The basic question underlying the field is how the properties and characteristics of a chemical entity (atom, ion, or molecule) are modified as it progresses from isolation to the condensed phase. The details of this transformation are very likely to be species dependent, but some major categories can be envisioned.

Clearly the kinds of interactions among neutrals are likely to be distinct from those between an ion and neutrals. Ionic clusters have long been studied by mass spectrometric techniques.<sup>1,2</sup> Because of the strong, attractive ion-neutral forces, ionic clusters play important roles in a variety of important processes including atmospheric chemistry,<sup>3</sup> cold plasma and combustion environments,<sup>4</sup> and obviously, solvation of ions in liquids.

Despite the extensive mass spectrometric work, the spectroscopy of ionic clusters by techniques (IR, VIS, UV, etc.) which directly yield structural information lags considerably behind such work on neutral clusters. Recently, however, there has been considerable progress in this arena as far as small clusters are concerned. Examples include low resolution IR work<sup>5</sup> on small, charged  $H_2O$  and  $NH_3$  clusters, as well as more recent higher resolution IR laser work<sup>6,7</sup> on species like  $H_5^+$ ,  $H_7^+$ ,  $H_9^+$ , and  $H_7O_3^+ \cdot H_2$ ,  $H_9O_4^+ \cdot H_2$ , and  $NH_4^+ \cdot (NH_3)_4$ . Visible laser induced fluorescence (LIF) has been reported<sup>8</sup> from ionic clusters, composed of one or two inert gas atoms attached to a fluorobenzene cation. In addition, there have been reports, particularly from the groups of Lineberger<sup>9</sup> and Lisy,<sup>10</sup> of visible and IR laser photodissociation work on larger ionic clusters, which yield some structural information, although the studies are



Availability Code	
Dist	Avail and/or Special
A-1	

of relatively low resolution

In this final report we describe (Section II) the construction and operation of a combined laser induced fluorescence and time-of-flight mass spectrometer apparatus. We shall refer to this device by the acronym LIFTOF. We shall then describe a series of experimental results obtained with the LIFTOF and the interpretation of the experimental data. Specific experiments to be discussed include ones involving  $\text{NO}^+$  complexes, monomer and dimer inert gas complexes with  $\text{C}_6\text{F}_6^+$  and their potential surface, and the evolution of the  $\text{C}_6\text{F}_6^+$  clusters from isolated ion to ion in a solid inert gas matrix.

## II. EXPERIMENTAL

### A. Apparatus

Fig. 1 shows an outline of the apparatus used for the experiment. A neutral precursor to the ion is seeded (~1% concentration) into the inert gas used for the supersonic expansion. This is accomplished either by on-line mixing of gases or passing the inert gas over a liquid or solid whose vapor pressure is controlled by its temperature. A homogeneous mixture is ensured by subsequent mixing in a length of 1/8" stainless steel tubing prior to expansion. The mixture is expanded through a .1 mm pinhole into the source chamber which is pumped by a large roots blower/mechanical pump combination with a pumping speed of 1200 CFM.

The ions are prepared within the expansion either by multi-photon ionization by ArF (193 nm) excimer laser radiation or by resonantly enhanced multi-photon ionization with the output of a YAG pumped dye laser as explained below.

For LIF experiments, an unfocussed, counterpropagating probe laser beam (Molelectron DL-II pumped by a Molelectron UV-24 nitrogen laser) enters from the opposite side of the source chamber via another Brewster's window and baffle, and crosses the expansion a few millimeters downstream. The undispersed fluorescence is collected by a 25 mm fl lens located 25 mm away from the intersection of the probe laser and jet, viewing in the direction orthogonal to both the expansion and laser axes. A photomultiplier tube and optical filter combination located outside the chamber is utilized to detect the fluorescence transmitted through a quartz window.

At about 15 to 20 mm downstream from the nozzle, a skimmer (Beam Dynamics UC-1, 0.58 mm orifice) samples the center portion of the free jet and provides a high degree of differential pumping between the source chamber and the main chamber, which is pumped by a 10" diffusion pump (Varian VHS-10) with a water cooled Chevron baffle. The base pressure in the main chamber is  $2 \times 10^{-7}$  torr. Immediately behind the skimmer is a small (25 mm thick), specially constructed sliding gate valve, which allows one to bring the source chamber up to atmospheric pressure for maintenance and adjustment while the main chamber remains isolated at high vacuum. The skimmer and nozzle assemblies are mounted on independent three-directional translation stages so that the alignment of the whole apparatus can be easily performed. Normally after the initial alignment, the position of skimmer in the directions perpendicular to the expansion axis is not disturbed. Only the separation of skimmer from the nozzle is adjusted.

The main chamber houses the base of a 125 cm long time-of-flight mass spectrometer. The design of the mass spectrometer follows the principles established by Wiley & McLaren.<sup>11</sup> One major difference of this design compared with a typical time-of-flight mass spectrometer is that the ions

are formed outside the "source" region at ground potential. The cations in the stream of the carrier gas are swept into the time-of-flight tube by applying a fast-rising pulse (typically +25V, 3  $\mu$ s duration) to the repeller plate. The second stage acceleration is achieved by floating the top plate and the whole flight tube at -330 VDC. It is found that a small positive voltage (0.5 V) applied to the center grid is very helpful in both resolution and sensitivity improvement. This is presumably due to the fact that any stray fields penetrating from the high negative potential nearby (within 1 cm) are compensated and the ions are confined in a smaller region prior to the arrival of the sweeping pulse.

The part of the time-of-flight tube which extends into the main chamber is surrounded by a cylindrical ground shield, with apertures to permit the passage of the skimmed supersonic ion beam. The drift tube is made from perforated stainless steel and supported by ceramic rings in a stainless steel housing. A small turbomolecular pump (Sargent Welch, 230 l/s) is attached to the housing to provide further differential and clean pumping. To achieve high sensitivity, a flight tube with large cross-sectional area (20 cm<sup>2</sup>) is used. The unwanted velocity component in the supersonic beam direction is corrected by a pair of deflection plates. An immersion ion lens is mounted about one third of the way up the drift tube to focus the ions onto the dual microchannel plate detector with a matched 50  $\Omega$  collector (Galileo FTD-2003). The current output is then amplified and fed into a LeCroy 9400 digital oscilloscope.

The data acquisition and timing control is performed by home-built hardware interfaced with an IBM-XT compatible microcomputer. A master oscillator running at 20 Hz fires the photoionization laser which ionizes the precursor molecule via a multi-photon process. After a short delay

(for helium 3 to 4  $\mu$ s), the probe laser is fired and the resulting signal from the photomultiplier tube is integrated and digitized and read into the computer for storage and further manipulation. The LIF signal is then averaged (typically 20 to 30 laser shots) and displayed on the screen. The laser grating is moved to the next position by a computer-controlled stepping motor and a new acquisition sequence is initiated.

The ion packet passes through the skimmer into the main chamber and arrives at the source region of the time-of-flight mass spectrometer at a delay of  $\sim 100$   $\mu$ s after the firing of the ionization laser. The repeller pulse is then applied and the LeCroy oscilloscope triggered. The ion flight waveform is accumulated and stored by the oscilloscope until the end of the LIF scan. Typically, several thousand waveforms are accumulated in this way. The entire TOF spectrum can be dumped to the microcomputer for permanent storage.

There is one feature that prevents our TOF mass spectrum from being a perfect measure of the relative cluster ion abundances. As the clusters grow quite large, the "outer" inert gas atoms are held together by only very weak inert gas atom-atom interactions. Such clusters are quite sensitive to collisional dissociation, literally a "flaking off" of the most weakly bonded inert gas atoms. Since we have employed high pressures in the reservoir (up to 20 atmospheres) to form the complexes, our vacuum in the TOF tube is probably not good enough to completely eliminate this effect at the highest expansion pressures. Some evidence of this effect is seen in slightly sloping baselines in the higher pressure TOF spectra, probably caused by collisional dissociation in the base of the TOF tube. Our belief is that this phenomenon has minimal consequences on our observations. It appears that the LIF spectrum is only very slightly



affected by these weakly bound inert gas atoms. Nonetheless, we are attempting to improve the pumping speed in the TOF tube to completely eliminate this effect in future measurements.

### III. RESULTS WITH $\text{NO}^+$ CLUSTER IONS

#### A. Background

A particularly effective way of creating clusters of metals, semi-metals, and other materials, has been to laser vaporize a solid sample of the metal just inside the throat of a supersonic expansion. This has led to the observation of large clusters of metals such as Al, Cu, Fe, Ni, W, etc. In addition, semiconductor clusters are well known and carbon clusters containing over 100 atoms have been observed and particular stability indicated<sup>12</sup> for  $\text{C}_{60}$ .

It is well known that in experiments of this type, the laser vaporization of the solid sample generates neutral clusters abundantly. In a number of experiments with such sources, a subsequent step of either electron or photon ionization was utilized to convert the neutral clusters to ionic ones for mass spectrometric analysis. In several of these experiments, considerable ambiguity has arisen concerning whether "magic numbers" observed for cluster ions were a property of the neutral clusters or the fragmentation processes and the ions' relative stabilities.<sup>13</sup>

The properties of ionic clusters are themselves most interesting, and it was recognized early on that the same laser vaporization sources that produced copious neutral clusters also produced some fraction of ionic clusters. In general, it is not clear whether the mechanism of ionic cluster formation involves gas-phase multi-photon or plasma ionization of neutral clusters, or direct desorption of charged species. However, once

produced, the ionic clusters can be conveniently studied by both ion cyclotron resonance and TOF techniques.

It is clear that, for many experiments, a more selective means of ionic cluster formation would be highly desirable. A technique would be to replace, for some cluster species, the relatively unselective laser vaporization of solid material, with the highly selective resonantly enhanced multi-photon ionization (REMPI) of gas phase molecules. Indeed, several investigators have observed ionic clusters derived from the REMPI of neutral van der Waals molecules found in supersonic free jet expansions (sometimes skimmed and sometimes not). The chief limitations of REMPI of neutral clusters include unknown, but likely substantial, fragmentation upon ionization and the inability to selectively ionize moderately large clusters. Indeed, often times it is extremely difficult to make large neutral clusters in the first place because of their extreme fragility.

We have developed a complementary technique to a number of those used previously. It incorporates some unique advantages. Our approach centers around the preparation of a nucleus for a cluster by the REMPI of an atom or molecule.

To make the discussion less abstract, we shall use by way of illustration the NO molecule, upon which our initial studies have centered. In these experiments, a few percent of NO is expanded in a He or Ar carrier gas. Just outside the throat of the supersonic jet, bare NO molecules are resonantly ionized in a 2+1 process. This REMPI of NO has been extensively studied.<sup>14-23</sup> For the isolated molecule, it is very selective and changing the dye laser wavelength  $\approx .01$  nm is sufficient to eliminate ion production. Similarly with the laser tuned to the resonance condition, it can be assumed with very high probability that the only ion being produced is  $\text{NO}^+$ .

Since the  $\text{NO}^+$  is produced very near to the nozzle's throat, it will undergo numerous collisions. Because of both the large collision cross section for charged species, as well as the very high binding energy of charged versus neutral clusters, it is easy to form clusters of the type  $(\text{NO})_x^+ \text{R}_y$  where R = rare gas.

We have previously used a similar technique for the laser induced fluorescence (LIF) study of aromatic organic ions and, more recently, have observed LIF spectra from the same ions with one or more rare gas atoms attached.<sup>24,25</sup> In the present experiments we have made two significant changes. Firstly, we have replaced the non-resonant or quasi-resonant ionization of an organic neutral with an excimer laser by the sharply resonant MPI of a small diatomic species. Secondly, we have modified our apparatus to include a skimmer for the expansion. The skimmed beam subsequently passes into a TOF mass spectrometer. The TOF allows a detailed study of the cluster species present, independent of whether they fluoresce or not. Further, it allows (in most cases) a precise determination of the coefficients x and y in the cluster formula  $(\text{NO})_x^+ \text{R}_y$ . We have found that reasonably large cluster species can readily be grown from such an expansion using  $\text{NO}^+$  as a seed. For example, we have observed clusters containing up to 4 NO molecules and 20 rare gas atoms.

#### B. Results and Discussion

For relatively low NO concentrations in the expansion, a time-of-flight mass spectrum such as is shown in Fig. 2 is obtained. Since the very broad mass range displayed in Fig. 2 is obtained by combining several successive scans over limited mass ranges, comparison of intensities, and hence inferred species abundances, from the lowest to the highest mass numbers is qualitative at best. However, an effort has been made to

normalize successive scans so that comparison of peak intensities within relatively narrow mass ranges is semi-quantitative.

As can be seen from the indicated identities of the peaks at the top of the Fig. 2, under conditions of low NO concentration, there are four dominant series,  $(\text{NO})_x^+ \text{Ar}_y$ , with  $x = 1, 2, 3$ , and 4. It can be seen from Fig. 2 that adducts with up to 15 Ar's are identified. In higher mass scans, under the same experimental conditions, we have observed up to 20 Ar atoms attached. As noted above, only very rough comparisons can be made across wide mass ranges, but from the Fig. 2 it is clear that there is a gradual fall-off in abundance in each  $(\text{NO})_x^+$  series as the number of Ar atoms increases. This certainly is to be expected; what is most surprising in this respect may simply be that one can form in this manner clusters with masses of order of 1000 amu from a single  $\text{NO}^+$  seed.

Another observation with respect to comparative abundances of cluster species can be made by following a  $(\text{NO})_x^+ \text{Ar}_y$  series with fixed  $y$ . Now with more reliability because of the narrower mass range, one can see again a gradual fall-off in intensity as the NO cluster size grows from  $x = 1-4$ .

The observations at low NO concentrations are not particularly unexpected. However as Fig. 3 shows, if the relative NO concentration in the expansion and the total backing pressure is increased, several interesting events occur. First,  $(\text{NO})_x^+ \text{Ar}_y$  clusters with much higher values of  $x$  are observed. Indeed, Fig. 3 is dominated by a  $(\text{NO})_x^+ \text{Ar}_y$  cluster series with  $y=0$  and  $x \leq 15$  even though Ar in the expansion is still in excess by a factor of greater than 25.

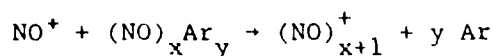
However what is probably most startling is the fact that for  $x \geq 8$  every  $(\text{NO})_x^+ \text{Ar}_y$  mass cluster, with  $x = \text{even}$  is less intense than either adjacent,

$x \pm 1 = \text{odd}$ , cluster. While not quite so dramatic, it appears that even for  $x \leq 7$ , the odd clusters are more favored. For relatively large clusters, the predominance of  $x = \text{odd}$  clusters is very striking. For example, one can dramatically see in Fig. 4 the odd even variations for  $(\text{NO})_x^+$  in the range  $x = 11$  to 15.

The fact that all of the  $(\text{NO})_x^+ \text{Ar}_y$  clusters are formed from an  $\text{NO}^+$  seed allows one to speculate upon the even-odd behavior of the clusters of pure NO. Previously when so-called "magic numbers" have been observed in cluster species, they have often been attributed to the "unique stability" of that species either as an ion or a parent neutral.

This could again be the explanation here. One can note that all even clusters of NO are potentially closed shell species while odd clusters must be open-shell molecules. Since  $\text{NO}^+$  is itself a closed shell ion, all species  $(\text{NO})_x^+$ ,  $x = \text{odd}$  are potentially closed shell while  $x = \text{even}$  must be open shell. Generally speaking, closed shell species are considered more stable than open-shell ones so that one might therefore expect the overabundance of odd  $(\text{NO})_x^+$  clusters.

While this explanation is facile, and certainly not disprovable, another, related explanation for the relative abundance of odd/even  $(\text{NO})_x^+$  is possible. Firstly, while the evidence is limited, there is no clear indication from the low NO concentration data, e.g. Fig. 2, that the potentially closed shell clusters of  $(\text{NO})_x^+ \text{Ar}_y$  with  $x = \text{odd}$  are overly abundant. In the richer NO expansions a substantial fraction of the NO is tied up in pure NO neutral clusters. From the closed/open shell arguments already advanced, one would expect the neutral  $(\text{NO})_x \text{Ar}_y$  with  $x = \text{even}$  to be more abundant than  $x = \text{odd}$ . These clusters may serve as precursors for large ionic clusters via the reaction,



with the Ar atoms carrying away the excess energy.

The stability of even sized neutral clusters thus favors the formation of odd sized ionic clusters. In support of this explanation, we note the well-known stability of  $(\text{NO})_2$  dimer, and our observation that for low NO concentrations the potentially closed shell clusters  $(\text{NO})_x^+ \text{Ar}_y$  with  $x = \text{odd}$  are not obviously more abundant than the open shell  $x = \text{even}$  ones.

Thus the overall predominance of odd  $(\text{NO})_x^+$  clusters could rest not with the special stability of  $(\text{NO})_x^+$  with  $x$  odd. Rather it alternatively can be explained by simple kinetic arguments and the likely stability of the NO dimer and higher even neutral clusters.

#### IV. RESULTS WITH $\text{C}_6\text{F}_6^+$ CLUSTER IONS

In addition to our  $\text{NO}^+$  cluster experiments, we have performed a large body of work on clusters of the hexafluorobenzene cation with inert gases, i.e.  $\text{C}_6\text{F}_6^+ \cdot \text{R}_n$  where  $\text{R} = \text{He}, \text{Ne}, \text{and Ar}$ . These experiments form an extremely valuable complement to the  $\text{NO}^+$  complex work. Unfortunately in the case of  $\text{C}_6\text{F}_6$ , the absorptions are so broad as to effectively render REMPI impossible so we have produced the ions by quasi-resonant 2-photon ionization with an ArF laser. Nonetheless it is likely that the dominant ion produced is uncomplexed  $\text{C}_6\text{F}_6^+$ .  $\text{C}_6\text{F}_6^+$  was chosen because of its well-known and easily observable LIF spectrum (see Fig. 5). It also is prototypical of ions with a moderately delocalized charge. Additionally, its condensed phase spectrum, in inert matrices, i.e. the limit of the cluster evolution, is well documented.

### A. He Clusters

Our results are best presented via a series of spectra, both LIF and TOF. Fig. 6 is the first of these spectra. It shows the LIF spectrum of the  $C_6F_6^+$  ion primarily as a function of He reservoir pressure. As the pressure is increased going from the bottom of Fig. 6 to the top, the predominant effect is an increase in the number and size of clusters,  $C_6F_6^+ \cdot He_n$ .

The traces with starred values of pressure also illustrate another method for increasing cluster size and concentration. The difference between a starred and an unstarred trace at the same reservoir pressure is the position of the photoionization laser with respect to the nozzle orifice. In the starred traces, the laser is moved closer to the orifice so that ions are created in a higher density region of the expansion and hence supposedly have more opportunities to form clusters. This supposition is verified by the near equivalence of the traces marked  $P_0 = 190^*$  and  $P_0 = 250$  in Fig. 6. Thus photoionization position and total reservoir pressure represent two nearly interchangeable parameters with which the experimenter can vary net He density at the point where the ion is created, the key factor in controlling cluster concentration and size.

By whichever method chosen, Fig. 6 illustrates how variation in cluster size affects the LIF spectrum. If we focus our attention on the region of the  $0_0^0$  band of  $C_6F_6^+$ , we note several cluster features growing in the region of the isolated ion origin. Under conditions in which  $C_6F_6^+$  is created at low He density, the only spectral features are the  $C_6F_6^+ 0_0^0$  line and a considerably weaker (~10%) satellite peak shifted  $38\text{ cm}^{-1}$  to lower frequency. The latter peak has previously been assigned<sup>8</sup> to the  $0_0^0$  band of

$C_6F_6^+ \cdot He$ . In the  $P_0 = 190$  trace of Fig. 6 and shown more clearly in Fig. 3, a weak progression in the van der Waals mode of  $C_6F_6^+ \cdot He$  is evident.

As the He density is increased, the sharp structure of the  $0_0^0$  bands of  $C_6F_6^+$  and  $C_6F_6^+ \cdot He$  are joined by a broader band; note the trace with  $P_0 = 250$ . The maximum of this band is roughly  $12 \text{ cm}^{-1}$  to the high frequency side of the  $0_0^0$  band of  $C_6F_6^+$ ; however, careful examination indicates that the origin of this band lies near the  $0_0^0$  band of  $C_6F_6^+ \cdot He$ , note top trace of Fig. 6.

At the highest He density two more cluster features appear distinctly. One is a relatively sharp structure, red shifted  $81 \text{ cm}^{-1}$  from the  $C_6F_6^+ 0_0^0$  band. The second feature is a second broad band of slightly narrower width than the first broad cluster peak. The maximum of the second peak is  $\sim 50 \text{ cm}^{-1}$  to the red of the first broad peak maximum.

In addition to the origin region of the  $C_6F_6^+$  LIF spectrum, Fig. 6 shows a scan extending to about  $500 \text{ cm}^{-1}$  higher frequency. The dominant transitions in uncomplexed  $C_6F_6^+$ , the  $0_0^0$ ,  $18_0^1$ , and  $17_0^1$  bands, are indicated in Fig. 6. There are, in addition, a few weaker bands, as evidenced in the lowest He density trace. All of these transitions have been previously assigned to the uncomplexed ion.<sup>26</sup> The key point of the overall spectrum is to demonstrate that the cluster features are essentially identical for all the vibrational transitions of the ion. Moreover, even the sharp spectral feature assigned to  $C_6F_6^+ \cdot He$  shows the same linewidth for the  $0_0^0$ ,  $18_0^1$ , and  $17_0^1$  bands of the complex. The  $\lesssim 2 \text{ cm}^{-1}$  linewidth for the  $17_0^1$  line indicates that the lifetime of the complex exceeds 5 psec., even though the energy content of  $\nu_{17}$  is more than a factor of two greater than the binding energy of the complex (see Section V.2). While this result is specifically applicable to  $C_6F_6^+ \cdot He$ , we have no evidence from the LIF spectra of



lifetime broadening due to the dissociation of any clusters,  $C_6F_6^+ \cdot R$ , containing excess internal energy from vibrational excitation. Thus we conclude that the cluster atoms are weakly coupled to the internal vibrational motions of the chromophore ion.

In Fig. 7, an expanded view of the  $0_0^0$  band region is shown. In these experiments the He density was varied by changing the position of the photoionization laser relative to the nozzle. The same cluster features evident in Fig. 6 are shown even more clearly in Fig. 7. In addition, Fig. 7 shows concurrent TOF mass spectra revealing the distribution of cluster ions under the conditions of the various LIF spectra. Fig. 7 indicates that in the low He density regime, the principal mass peaks in the TOF spectrum belong to  $C_6F_6^+$  and  $C_6F_6^+ \cdot He$ . Furthermore, the relative intensities of  $C_6F_6^+ / C_6F_6^+ \cdot He$  in the LIF and TOF spectra are comparable. This statement is true whether one compares peak or integrated intensities as the isolated and clustered ion linewidths are essentially the same.

As the He density increases, cluster peaks  $C_6F_6^+ \cdot He_n$  with  $n \approx 2-6$  appear in the TOF spectrum. At the same time, the broad cluster feature in the LIF spectrum grows in. There are at least three important observations related to that growth. (i) The integrated intensity (relative to the isolated ion) of the broad LIF peaks far exceeds the integrated intensity of the  $n \approx 2-6$  cluster peaks in the TOF spectrum. This point is illustrated semi-quantitatively in Table I. (ii) There are no peaks in the LIF spectrum in the region of the  $C_6F_6^+ \cdot He_2$  transition, until TOF peaks for  $n \approx 4-6$  (top trace Fig. 7) are developed. (iii) The lower frequency broad cluster peak in the LIF spectrum appears to be the dominant cluster feature at highest cluster size. However, its red shift is less than that of the sharp line LIF spectrum attributed to the cluster  $C_6F_6^+ \cdot He_2$ . It is also

less than the reported electronic shift of the LIF spectrum of  $C_6F_6^+$  observed in a solid Ne matrix.<sup>26</sup> (While a solid He matrix experiment has, of course, never been performed, an extrapolation of a large body of work in heavier rare gas matrices would predict that a He matrix shift would be even smaller than a Ne matrix shift.) The results of our LIF observations are summarized in Table II.

A final point should be made about the TOF spectra in Fig. 7. They show only the mass region  $m \approx 180-210$ . No significant peaks were observed below  $m = 186$ , i.e.  $C_6F_6^+$ . At masses above 210, the only additional peaks observed can be identified as belonging to species of the form  $(C_6F_6)_m^+ \cdot He_n$ . Such species involving multiple benzenoid groups are considered in detail later in this paper. It suffices here to note that species with  $m > 1$  appear to make no contributions to any of LIF spectra observed.

#### B. Ne Clusters

Fig. 8 shows the development of  $C_6F_6^+ \cdot Ne$  clusters as monitored by both the LIF and TOF spectra. In this case, cluster formation was promoted by increasing the Ne (actually a mixture of 90% Ne/10% He) pressure in the reservoir. The TOF scale is now expanded to show not only neat ion-Ne clusters but also the region of the dimer, trimer, etc. fluorobenzene cation mass peaks, i.e.  $(C_6F_6)_m^+ \cdot Ne_n$ . Overall, the Ne cluster development parallels that of the He clusters, but it does differ in detail.

At the lowest Ne density trace in Fig. 8, the TOF spectrum already shows a weak Ne adduct peak with  $n = 1$  and  $(C_6F_6)_m^+$  peaks with  $m = 1-3$ . At slightly increased  $P_0$ , the LIF spectrum shows a clearly defined  $0_0^0$  band for  $C_6F_6^+ \cdot Ne$ , red shifted  $56 \text{ cm}^{-1}$  from  $0_0^0$  of  $C_6F_6^+$ , and a progression of sharp lines in a van der Waals mode. There appear also clearly TOF peaks for  $n \approx 1-6$ , and a broad cluster structure in the LIF spectrum. This structure, as

in the He complex spectrum, has its maximum to the blue of the  $0_0^0$  band of  $C_6F_6^+$  but its origin appears to roughly coincide with the  $C_6F_6^+ \cdot Ne$  origin. Interestingly, under these conditions while the TOF spectrum indicates ample  $C_6F_6^+ \cdot Ne_2$ , there is no discernible structure at twice the  $C_6F_6^+ \cdot Ne$  red shift, i.e. the region of the LIF spectrum where the origin of  $C_6F_6^+ \cdot Ne_2$  might be expected.

At the highest Ne densities, the TOF spectrum indicates the mass distribution of the mono fluorobenzenoid clusters,  $C_6F_6^+ \cdot Ne_n$  maximizes with  $n \approx 8$  but clearly extends to  $n$  approximately twice this number. In addition, there appear peaks attributable to polymer fluorobenzenoid clusters,  $(C_6F_6)_m^+ \cdot Ne_n$  with  $m = 2, 3, \dots$  and  $n$  values from  $0 \sim 10$ .

All sharp structure, save a weak, uncomplexed  $C_6F_6^+ 0_0^0$  band, has vanished from the corresponding LIF spectrum. At the same time, several broad bands have developed. At even higher Ne density (not shown), the strongest broad peak in the top trace of Fig. 8 becomes clearly dominant. The position of this peak, i.e. red-shifted by  $-56 \text{ cm}^{-1}$ , agrees well with the reported Ne matrix red shift of  $C_6F_6^+$  of  $58 \text{ cm}^{-1}$ , as is indicated in Fig. 8. This dominant peak is flanked by two more broad peaks, one  $-46 \text{ cm}^{-1}$  further to the red and the other roughly  $40 \text{ cm}^{-1}$  to the blue. The  $C_6F_6^+ \cdot Ne_n$  LIF results are summarized in Table II.

### C. Ar Clusters

The TOF and LIF spectra of  $C_6F_6^+ \cdot Ar$  clusters are correlated in Fig. 9. The general appearance of the spectra is maintained from the clusters of the lighter inert gases, but again the spectra differ in detail. In this experiment, cluster size is controlled by the percent of Ar in a He expansion.

In the lowest Ar density expansion, the TOF spectrum shows substantial

population for the clusters  $C_6F_6^+ \cdot Ar_n$  with  $n = 1-5$ . The corresponding LIF spectrum shows a very complicated series of sharp lines in addition to the  $0_0^0$  band of  $C_6F_6^+$ . These lines can be shown to completely vanish upon total removal of Ar. They have been assigned<sup>25</sup> (but not analyzed) to  $C_6F_6^+ \cdot Ar$  and  $C_6F_6^+ \cdot Ar_2$  which show red shifts in the  $0_0^0$  band relative to the  $C_6F_6^+$  spectrum of  $420\text{ cm}^{-1}$  and  $785\text{ cm}^{-1}$ , respectively.

In addition to the sharp structure, there is also already present in the 3% Ar trace, a broad structure in the LIF spectrum. Like the lighter rare gas clusters, the broad structure shows an onset in the vicinity of the  $0_0^0$  band of the one Ar adduct of  $C_6F_6^+$  but its maximum is again shifted to much higher frequencies. However, unlike the cases of He and Ne, the Ar cluster broad structure maximum remains to the red of the  $C_6F_6^+ 0_0^0$  band. This red shift is roughly  $110\text{ cm}^{-1}$  for an 8% Ar mix where the cluster size ranges up to  $n \approx 10$ , but whose mean  $n$  value is about 4.

As the Ar density is increased to 14 and 21%, the TOF spectra show a clear shift to higher Ar cluster sizes with mean values of  $n \approx 5$  and 7 and maximum  $m$  values two to three times as great. The corresponding LIF spectra show no sharp structure, save a weak and nearly vanishing  $C_6F_6^+ 0_0^0$  band. However, the dominant broad band of the spectrum both sharpens and shifts as the average Ar cluster size increases. In our highest Ar density spectrum, the red shift of this band is indistinguishable from the red shift<sup>14</sup> of  $C_6F_6^+$  in an Ar matrix,  $255\text{ cm}^{-1}$ .

In addition to the dominant band, two other broad bands appear in the LIF spectrum of Fig. 9. The highest frequency band is simply the dominant cluster band analog from the  $18_0^1$  transition and represents nothing new. However, the most red shifted band ( $\sim 425\text{ cm}^{-1}$ ) is new, associated with the  $0_0^0 C_6F_6^+$  transition, and clearly much more red shifted (approximately

twice) than the matrix value. These LIF results are summarized in Table II.

#### D. $(C_6F_6)_m^+$ Polymer Cluster

It is not surprising that in the TOF mass spectra, we observe masses corresponding to what we call polymer fluorobenzenoid clusters  $(C_6F_6)_m^+$  and  $(C_6F_6)_m^+ \cdot R_n$ . It is an important question as to whether these polymer clusters are the carriers of any of the LIF spectra, particularly the broad ones. Fig. 10 shows correlated TOF and LIF spectra as a function of  $C_6F_6$  neutral concentration in the jet. This variation was accomplished by changing the temperature of the  $C_6F_6$  container and hence its partial pressure in the expansion.

As would be expected and shown by the TOF spectra of Fig. 10, higher partial pressures of  $C_6F_6$  favor the formation of higher polymers  $(C_6F_6)_m^+$  and  $(C_6F_6)_m^+ \cdot R_n$ . It has been speculated that the broad structures observed in the LIF spectra may be associated with these polymers. However as Fig. 10 clearly shows, as the number of polymers increase in the TOF spectra, the strength of the broad LIF band decreases. Indeed, one finds rather that the strength of the LIF band correlates with the population of the higher n clusters,  $C_6F_6^+ \cdot Ar_n$ . As these clusters disappear in the TOF spectrum due to increased polymer formation at higher  $C_6F_6$  density, so does the intensity of the broad structure in the LIF spectrum decrease.

While the results shown in Fig. 10 were obtained for an 8% Ar/He expansion, experiments varying the partial pressure of  $C_6F_6$  in He and Ne provided very similar results with respect to the broad structures in their LIF spectra. We conclude from the TOF data that the broad structures in the LIF spectra are due solely to monomer fluorobenzenoid clusters of the form  $C_6F_6^+ \cdot R_n$ .

## V. DISCUSSION

### A. Cluster Characteristics

There is now a rather large body of data concerning fluorobenzenoid-rare gas ionic complexes,  $(C_6F_6)_m^+ \cdot R_n$ . Unlike TOF spectra, the LIF spectra provide us with a window through which to view the cluster's geometric structure. On the other hand, the TOF spectra serve the critical function of literally labeling the room (cluster) of the window through which we're looking.

In this section, we wish to speculate upon a model of cluster growth. Unlike the experimental data, the validity and/or uniqueness of the model is open to question. However, we would hasten to add that the model proposed adequately accounts for all the observations.

Our approach to the problem of building a model which is consistent with the experimental observations is to first reduce them to a small number of characteristics which the clusters have been shown to possess. We divide these characteristics into three categories: 1. general -- applying to all observed clusters, 2. sharp line -- applying to those cluster structures giving rise to sharp line LIF spectra, and 3. broad line -- applying to those cluster structures giving rise to broad line LIF spectra.

#### 1. General

Probably the only observation that is generally applicable to all the observed LIF spectra is that the carrier is always a monomeric benzenoid cluster of the form  $C_6F_6^+ \cdot R_n$ . This conclusion seems inescapable from the combined LIF and TOF observations wherein the partial pressure of  $C_6F_6$  in the expansion was varied.

## 2. Sharp Line Clusters

The structures proposed for the clusters giving rise to the sharp LIF spectral transitions will have to be consistent with the following observations:

- a. The one-atom adduct,  $C_6F_6^+ \cdot R$  where  $R = He, Ne, \text{ and } Ar$  all show sharp structures, including a low frequency vibrational progression involving predominantly movement of the adduct atom with respect to the ring of the cation.
- b. There appear at least for the cases of  $R = He$  and  $Ar$ , a second series of sharp LIF spectra ascribable to  $C_6F_6^+ \cdot R_2$  with spectral red shifts approximately twice those ascribed to the  $C_6F_6^+ \cdot R$  species. However, it appears that the yield for producing the  $C_6F_6^+ \cdot R_2$  species showing sharp LIF structure, is relatively low in our expansion.
- c. The red shifts of the spectra attributable to  $C_6F_6^+ \cdot R$  are comparable to the red shift for  $C_6F_6^+$  in the corresponding solid matrix. The corresponding red shifts for  $C_6F_6^+ \cdot R_2$  are much larger than the matrix values.
- d. The relative intensity of the peaks in the LIF and TOF spectra correlate well for the  $C_6F_6^+$  and  $C_6F_6^+ \cdot R$  species, but  $C_6F_6^+ \cdot R_2$  peaks are clearly evident in the TOF spectra at low densities where corresponding  $C_6F_6^+ \cdot R_2$  sharp line structure in the LIF spectra is absent.
- e. Lack of spectral line broadening on the cluster peaks associated with vibrational excitation energies (in excess of  $R$  bonding energies), of the chromophore  $C_6F_6^+$  indicate relatively long cluster lifetimes and weak coupling between the internal  $C_6F_6^+$  vibrations and the cluster modes.

### 3. Broad Line Clusters

The characteristics of the clusters associated with the broad LIF lines include the following:

- a. All inert gas species  $C_6F_6^+ \cdot R_n$  show clearly defined, but broad ( $50 \text{ cm}^{-1} \lesssim \Delta\nu \lesssim 300 \text{ cm}^{-1}$ ) LIF structures. These structures initially appear under conditions where the TOF spectra indicate predominantly small clusters ( $n$  values mostly  $\lesssim 6$ , and cluster distribution maxima as low as  $n \approx 3$ ).
- b. The most blue shifted broad peak has its maximum to the blue of the  $0_0^0$  band of  $C_6F_6^+$  for He and Ne, and just to the red for Ar. However, the origin of this broad peak appears to be in the same spectral region as the transition from the species  $C_6F_6^+ \cdot R$  for all the inert gases.
- c. With Ne and Ar where comparisons are possible, the red shift of the dominant broad LIF peak maximum at highest cluster sizes coincides very well with the red shift of  $C_6F_6^+$  in the corresponding inert gas matrix. There is some evidence that this peak sharpens as the cluster size grows.
- d. There is evidence of a weaker broad LIF peak to the red of the dominant surviving peak.
- e. The integrated intensity of the broad LIF spectral peaks ratioed to that of the uncomplexed ion  $C_6F_6^+$  far exceeds the corresponding ratio in the TOF spectrum for all the  $C_6F_6^+ \cdot R_n$  peaks. The result argues that the broad LIF peaks must be at least in part homogeneously broadened.

#### B. Sharp Line Model

##### 1. General Characteristics

The structure of the clusters giving rise to the sharp LIF lines is relatively straightforward to ascertain for several reasons. In the first



place, it appears that this structure can be ascribed entirely to the simplest clusters  $C_6F_6^+ \cdot R$  and  $C_6F_6^+ \cdot R_2$ . Secondly, their structure is likely analogous to those previously deduced for neutral van der Waals clusters involving aromatic systems and inert gases. However, it is necessary to fully appreciate the structure of these clusters before any progress can be made towards the understanding of the more complex structures associated with the broad LIF transitions. In addition, while there are strong parallels with similar neutral van der Waals structures, there are also some differences which are important to point out.

We believe that the monomer and dimer inert gas complexes responsible for sharp LIF transitions are formed respectively by placing first an inert atom above the plane of the ring and centered on the  $C_6$  symmetry axis. In the  $C_6F_6^+ \cdot R_2$  complexes the second adduct atom then occupies the equivalent bonding position on the  $C_6$  axis below the ring, as shown in Fig. 11. These structures account for all the sharp line spectra characteristics a and b given above. It is probably the only reasonable structure explaining the approximate additivity of the red shifts for the  $R_1$  and  $R_2$  species. This assignment for the carriers of the sharp LIF lines is indicated in Table II. It should also be noted that the cluster progressions in  $C_6F_6^+ \cdot He$  and  $C_6F_6^+ \cdot Ne$  can be adequately explained using a model potential wherein this configuration was at the minimum, as described in the following section, V.B.2.

This structure is also very consistent with observation e which indicates that weak coupling occurs between modes  $17_0^1$  and  $18_0^1$  and the cluster bond. Since  $\nu_{17}$  and  $\nu_{18}$  are in-plane cation modes, physically one would expect little coupling to atoms located above and below the plane.

This model does not provide a complete explanation for the magnitude

of the red shift (characteristic c) nor the anomalous behavior of the intensities of the correlated LIF and TOF spectra of  $C_6F_6^+ \cdot R_2$ . However, the model is not inconsistent with either of these observations.

The magnitudes of the red shifts are large compared both to those observed for similar neutral van der Waals complexes and compared to the matrix value. With respect to the former point, Table III lists the average red shift for several similar neutral van der Waals species and for the cluster ions,  $C_6F_6^+ \cdot R$ . The shift of the ions is in general almost an order of magnitude larger. However, this result is not particularly surprising. For the  $C_6F_6^+ \cdot R$  species, a charge induced dipole interaction is introduced into the potential. This term is expected to yield a considerably stronger bond in both the ground and excited state compared to the neutral complexes. Thus it is not unexpected that the difference in these bonds, i.e. roughly the red shift, increases proportionally in size also. Thus, we take the view that the red shifts observed for  $C_6F_6^+ \cdot R_1$  and  $C_6F_6^+ \cdot R_2$  are expected in terms of a cation-inert-gas potential. The fact that the red shifts are considerably larger than the ones observed for  $C_6F_6^+$  in the corresponding matrices, we leave as a problem for the larger cluster structures to explain.

## 2. $C_6F_6^+ \cdot He$ Potential

While the preceding section has given us a good qualitative picture of the structure of the  $C_6F_6^+ \cdot R$  (and  $R_2$ ) species, it has provided little quantitative information concerning the pair-wise potential between an ion and an inert gas. For this information, we can turn to the vibrational frequencies measured for the inert gas atom's motion relative to the charged ring. Tables IV and V list respectively the experimental vibrational intervals obtained for  $C_6F_6^+ \cdot He$  and  $C_6F_6^+ \cdot Ne$ . The spectra from

which these intervals were obtained are shown in Fig. 12.

The information in Tables IV and V can be used to test and refine model potentials for the complex. Jortner *et al.*<sup>27</sup> have proposed a potential for systems of this type, consisting of a sum of pairwise Lennard-Jones 12-6 interactions for the helium atom with the carbon and fluorine atoms:

$$V_{LJ}(r_{He}) = \sum_i A_i \left\{ \frac{-1}{r_{iHe}^6} + \frac{(r_{iHe}^0)^{6/2}}{r_{iHe}^{12}} \right\} \quad (1)$$

$$\text{where } r_{iHe} = |r_i - r_{He}| \quad (2)$$

and a charge-induced dipole term describing the interaction of the distribution of the net positive charge on the  $C_6F_6^+$  ion with the polarizability of the helium atom:

$$V_{cid}(r_{He}) = - \frac{\alpha_{He} e^2}{2} |F(r_{He})|^2 \quad (3)$$

$$\text{where } F_{\xi} = \sum_i \frac{(ei/e)}{r_{iHe}^3} (\xi_i - \xi_{He}); \xi = x, y, z \quad (4)$$

The total potential:

$$V_{tot}(r_{He}) = V_{LJ}(r_{He}) + V_{cid}(r_{He}) \quad (5)$$

$$= V(x, y, z) \quad (6)$$

is a function of three spatial variables which were chosen as  $z$ , the height of the helium atom above the ring, and the orthogonal displacements  $(x, y)$  of the atom from the  $C_6$  axis through the center of the ring. The  $x$  axis was chosen to lie  $15^\circ$  from the direction of a C-F bond, so that the potential cuts  $V(x, 0, z)$  and  $V(0, y, z)$  are identical.

If the  $C_6F_6^+$  ring is assumed to be infinitely massive compared to the helium atom, the Hamiltonian describing the motion of the atom relative to the fixed ring may be written as:

$$H = \frac{\hbar^2}{2m_{\text{He}}} \left[ \frac{d^2}{dx^2} + \frac{d^2}{dy^2} + \frac{d^2}{dz^2} \right] + V(x,y,z) \quad (7)$$

The assumption is also made that the  $C_6F_6^+$  chromophore may be treated as a rigid body. This assumption is supported by the observation that the cluster spectra associated with different vibrational levels of  $C_6F_6^+(\bar{B})$  are identical.

Plots of the total potential,  $V(x,y,z)$ , with reasonable values for the various parameters show two interesting features (see Fig. 13). First, the minimum is located above the center of the ring, and secondly, the minimum energy path for moving the helium atom away from the  $C_6$  axis keeps the height of the atom above the ring approximately fixed at the equilibrium value for quite substantial displacements. The Hamiltonian (7) may usefully be expressed as the sum:

$$H = H_s(z) + H_b(x) + H_b(y) + \Delta V(x,y,z) \quad (8)$$

where the "stretching" Hamiltonian:

$$H_s(z) = \frac{\hbar^2}{2m_{\text{He}}} \frac{d^2}{dz^2} + V_s(z), \quad V_s(z) = V(0,0,z) \quad (9)$$

the "bending" Hamiltonian:

$$H_b(x) = \frac{\hbar^2}{2m_{\text{He}}} \frac{d^2}{dx^2} + V_b(x), \quad V_b(x) = V(x, 0, z_m) \quad (10)$$

( $z_m$  is such that  $\left[\frac{dV_s}{dz}\right]_{z=z_m} = 0$ , i.e.  $z_m$  is the height of the atom above the ring at the minimum of the stretching potential),  $H_b(y)$  is similar to  $H_b(x)$ , and:

$$\Delta V(x, y, z) = V(x, y, z) - V_s(z) - V_b(d) \quad (11)$$

where  $|d| = (x^2 + y^2)^{1/2}$ . The determination of the vibrational energy levels for the model potential  $V(x, y, z)$  now breaks down into three stages:

(a) Calculation of the zeroth order stretching and bending vibrational energy levels and wavefunctions by numerically solving the separated Schrödinger equations for the vibrational coordinates  $z$  and  $s$  (or  $y$ ):

$$\left[ \frac{\hbar^2}{2m_{\text{He}}} \frac{d^2}{dz^2} + V_s(z) \right] X_s(z) = E_s X_s(z) \quad (12)$$

and

$$\left[ \frac{\hbar^2}{2m_{\text{He}}} \frac{d^2}{dx^2} + V_b(x) \right] X_b(x) = E_b X_b(x) \quad (13)$$

These equations were solved by using the Numerov-Cooley algorithm.<sup>28</sup>

(b) Evaluation of the first order corrections,  $E'$ , to the combined stretching and bending energy levels due to the difference potential perturbation,  $\Delta V$ :

$$E' = \langle s \ b_1 \ b_2 | \Delta V | s \ b_1 \ b_2 \rangle \quad (14)$$

where

$$(s \ b_1 \ b_2) = X_s(z) X_{b_1}(x) X_{b_2}(y) \quad (15)$$

The required matrix elements were evaluated by three dimensional numerical quadrature using Gauss-Legendre weights and abscissae, up to 192 x 192 x 192 points were employed to ensure convergence.

(c) Evaluation of the off-diagonal matrix elements of  $\Delta V$ :

$$\Delta V^{mn} = \langle s^m \ b_1^m \ b_2^m | \Delta V | s^n \ b_1^n \ b_2^n \rangle \quad (16)$$

followed by the construction and diagonalization of the numerically generated Hamiltonian matrix. The matrix elements were again computed by three dimensional Gauss-Legendre quadrature. Symmetry considerations show that off-diagonal matrix elements with  $\Delta b_1$  and/or  $\Delta b_2$  odd must be zero. For levels which are doubly degenerate through first order -  $(s \ b_1 \ b_2)$ ,  $(s \ b_2 \ b_1)$ ,  $b_1 \neq b_2$ , symmetric and antisymmetric combinations can be formed:

$$\frac{1}{\sqrt{2}} [(s \ b_1 \ b_2) + (s \ b_2 \ b_1)] \ \& \ \frac{1}{\sqrt{2}} [(s \ b_1 \ b_2) - (s \ b_2 \ b_1)]$$

The transitions observed in the fluorescence excitation spectrum from the vibrationless level of the ground state must be to totally symmetric vibrational levels of the excited state. These levels are constructed from the singly degenerate basis functions  $(s \ 0 \ 0)$  and  $(s \ 2b_1 \ 2b_1)$ , together with the symmetric combination of the stretch-bend functions with both  $b_1$  and  $b_2$  even, i.e.  $1/\sqrt{2}[(s \ 2b_1 \ 2b_2) + (s \ 2b_2 \ 2b_1)]$ . The Hamiltonian matrix for these levels is set up, including basis functions up to a fixed energy above  $(0 \ 0 \ 0)$  and diagonalized.

The energies obtained at the different stages in the calculation are

reported in Table IV, together with the experimental results for comparison. The parameters used in generating the model potential were obtained from various sources. The geometry of  $C_6F_6^+$  ( $\bar{B}$ ) was assumed to be the same as for the ground state of neutral  $C_6F_6$ ,  $r_{CC} = 1.394$  Å, determined by electron diffraction.<sup>29</sup> The polarizability of the He atom is  $\alpha_{He} = 0.204956 \times 10^{-24}$  cm<sup>3</sup>.<sup>30</sup> The Lennard-Jones parameters for C-He and F-He were extrapolated from those used for previous model calculations on aromatic-rare gas systems,<sup>31</sup>  $A_C = 4000$  cm<sup>-1</sup>,  $r_{CHE}^\circ = 3.3$  Å,  $A_F = 3800$  cm<sup>-1</sup>,  $r_{FHE}^\circ = 3.2$  Å. The net positive charge on the  $C_6F_6^+$  ion was distributed according to the scheme proposed by Jortner *et al.*,<sup>27</sup>  $e_{Ce} = 1/6$ ,  $e_{Fe}/e = 0$ . Basis functions up to 120 cm<sup>-1</sup>, above the (0 0 0) level were included in the construction of the full Hamiltonian matrix.

The comparison of the calculations with the experimental results is quite appealing. The most obvious discrepancy is that the bending level (002) + (020) is predicted to lie below the stretching level (100), while the experimental results suggested the reverse order. Attempts at reversing the order predicted by theory through variations in the four Lennard-Jones parameters have so far proved to be unsuccessful. A relatively small shift of the zeroth order levels is required; once (100) is below (002) + (020) the substantial Fermi resonance between these levels will push (002) + (020) up still further. The calculations did reveal the anticipated Fermi resonance between the pairs of levels, (100) with (002) + (020) and (200) with (004) + (040), through which transitions to the bending levels borrow intensity from the allowed stretching progression. Inspection of the eigenvector coefficients obtained by diagonalization of the Hamiltonian matrix showed that there was also substantial mixing of (002) + (020) with (102) + (120) and of (004) + (040) with (104) + (140).

It is believed that these mixings reflect the fact that there is a tendency for the height of the He atom above the ring to decrease as it moves away from the center (see the contour plot of the potential in Figure 13). In the limit the He atom may orbit the ion, making the method used in these calculations inadequate.

The minimum of the model potential described in the text above is located 2.43 Å above the plane of the ring; the equilibrium well depth is 136 cm<sup>-1</sup>. The energies of the vibrational levels we have observed amount to a very substantial fraction of the well depth, and the potential surface is extensively sampled. The red shift of the cluster origin leads to the conclusion that the well depth for C<sub>6</sub>F<sub>6</sub><sup>+</sup>( $\bar{X}$ )...He is about 40 cm<sup>-1</sup> shallower than for C<sub>6</sub>F<sub>6</sub><sup>+</sup>( $\bar{B}$ )...He, indicated a well depth of -100 cm<sup>-1</sup> for C<sub>6</sub>F<sub>6</sub><sup>+</sup>( $\bar{X}$ )...He.

### 3. C<sub>6</sub>F<sub>6</sub><sup>+</sup>•Ne and C<sub>6</sub>F<sub>6</sub><sup>+</sup>•Ar Potentials

In addition to C<sub>6</sub>F<sub>6</sub><sup>+</sup>...He, a number of other ion-atoms and ion-molecule complexes containing the C<sub>6</sub>F<sub>6</sub><sup>+</sup> chromophore have been investigated. Table V tabulates the results for C<sub>6</sub>F<sub>6</sub><sup>+</sup>...Ne obtained experimentally, and also gives the results of a calculation of the vibrational energy levels (parameters - A<sub>C</sub> = 11100 cm<sup>-1</sup>, r<sub>C</sub><sup>o</sup> = 3.49 Å, A<sub>F</sub> = 5000 cm<sup>-1</sup>, r<sub>F</sub><sup>o</sup> = 3.30 Å, α<sub>Ne</sub> = 0.395 x 10<sup>-24</sup> cm<sup>3</sup>, these give a well depth of -210 cm<sup>-1</sup>, with the Ne atom 2.66 Å above the ring). The match between experiment and theory is again appealing, suggesting that the model potential constructed from considerations of the purely physical interactions within the complex provides a useful description of the system.

The preliminary conclusions from the spectra of C<sub>6</sub>F<sub>6</sub><sup>+</sup>...Ar are that the dramatic increase in the red shift on going from He (37.5 cm<sup>-1</sup>) or Ne (57.4 cm<sup>-1</sup>) (420 cm<sup>-1</sup>) to Ar, and the observed increase in the stretching



vibrational spacing to  $\sim 66 \text{ cm}^{-1}$  indicate that the binding between an Ar atom and  $\text{C}_6\text{F}_6^+$  ( $\tilde{\text{B}}$ ) is much stronger than for the lighter rare gases. Model calculations of the type developed for  $\text{C}_6\text{F}_6^+ \cdots \text{He}$  support this conclusion, using reasonable values for the Lennard-Jones parameters and the known polarizability of the Ar atom,<sup>30</sup> the stretching frequency is grossly underestimated (calculated  $44 \text{ cm}^{-1}$ ). The increased strength of the attractive interactions between Ar and  $\text{C}_6\text{F}_6^+$  ( $\tilde{\text{B}}$ ), compared to the essentially physical binding of the lighter rare gases to this ion, arises from the development of some charge transfer bonding in the  $\text{C}_6\text{F}_6^+ \cdots \text{Ar}$  complex, which is facilitated by the lower ionization potential of Ar relative to He and Ne.

### C. Broad Line Model

We now wish to propose a structure for the complexes,  $\text{C}_6\text{F}_6^+ \cdot \text{R}_n$  which account for the broad lines in the LIF spectra. This model is necessarily appropriate for the larger cluster species and ultimately must reach the matrix limit. It also must interface with the structure proposed above to explain the sharp line spectra from  $\text{C}_6\text{F}_6^+ \cdot \text{R}$  and  $\text{C}_6\text{F}_6^+ \cdot \text{R}_2$ .

We begin by noting that whenever there exists a species  $\text{C}_6\text{F}_6^+ \cdot \text{R}_n$ ,  $n \geq 2$ , there are two very distinct structural isomers possible. We will illustrate with the simple case of  $n = 4$ . In that case, we have for one isomer the structure depicted in Fig. 14 and clearly derived from the structure (Fig. 11) described above as accounting for part of the sharp line structure. We shall refer to the structure in Fig. 11 as the closed-face-sandwich (CFS) structure.

Another distinct structural possibility is for all the inert gas atoms to be on the same side of the ring, and to share the cation's charge roughly equally. This structure we call the open-faced-sandwich (OFS)

structure and is depicted in Fig. 15.

For the smallest clusters, i.e.  $n = 2$ , the OFS is very likely thermodynamically less stable than the CFS, since in the latter structure the atoms are placed at the primary minima of the potential. On the other hand, there is no absolute requirement for the obtainment of thermodynamic equilibrium between these two configurations in the jet, especially since moving an atom from one side of the ring to the other should guarantee a significant potential barrier between the two isomers. Thus in the jet, the relative population of these species will probably be more determined by dynamic rather than thermodynamic considerations.

In any case, the relative stabilities of the larger clusters, e.g. as pictured in Figs. 14 and 15, likely become relatively close. For those species, a CFS for larger  $n$  would require approximately  $n/2$  R's on each side of the ring arranged in approximately symmetric patterns, but with the assumption that one atom continued to occupy the primary  $C_6$  axis location on each side. The OFS would require all  $n$  R's on the same side of the ring. Clearly as the clusters grow large, the true OFS structure becomes statistically less and less probable.

For larger  $n$ , other isomers become possible. If  $n-1$  atoms are on one side and one on the other, the latter atom would naturally lie on the  $C_6$  axis. We denote this structure as 1R-OFS. Accordingly, if a substantial number of atoms are on each side, but none occupying the  $C_6$  axis position, we shall call the structure the closed open faced sandwich (COFS).

Let's now see if these structures can explain the characteristics of the broad LIF spectral lines. It is probably best to begin with the issues remaining from the sharp line model. Firstly, we have the definite appearance of species  $C_6F_6^+ \cdot R_2$  in the mass spectrum under conditions where

no hint appears of the LIF spectrum of the symmetrical CFS structure.

We believe that the extra intensity of the TOF peak originates from the OFS structure. The LIF spectrum of the OFS is rather interesting to speculate upon. In the first place, its red shift is probably much less than the CFS, in the simplest approximation only one-half the CFS since roughly two half strengths ion-R bonds are formed. This analogy would place the red shift of the OFS near that of  $C_6F_6^+ \cdot R$ , which is indeed consistent with the experimental observations.

We believe that the origin of the first broad band to appear as the cluster size increases (characteristic b) is then attributable primarily to OFS  $C_6F_6^+ \cdot R_n$  ( $n \geq 2$ ). OFS  $C_6F_6^+ \cdot R_n$  with  $n > 2$  then lie in about the same spectral region as  $C_6F_6^+ \cdot R_2$  and inhomogeneously broaden and strengthen its LIF peak.

As mentioned in characteristic 3.e, all of the broadening cannot be heterogeneous. There are two clear mechanisms to explain the remaining broadness of the structure. A comparison of the cluster progression of the  $C_6F_6^+ \cdot R$  species with the contour of the broad peak suggests that similar, but unresolved vibrational structure of the OFS  $C_6F_6^+ \cdot R_n$ ,  $n \geq 2$  structure is the dominant mechanism accounting for the broadness of the transition. The distinct displacement of the band maxima from their origins would indicate that the Franck-Condon factors have become distinctly less diagonal for the OFS compared to the CFS structure. Some additional inhomogeneous broadening may result from hot bands of the modes involving the R's.

Based upon the relative paucity of different n in the TOF distributions and the intensity data presented in Table I, we suspect that the observed, featureless LIF contours must also have their individual

vibrational transitions homogeneously broadened. This broadening may be explained in analogy with recent work<sup>32,33</sup> on neutral clusters as arising from the nearly fluid state of the OFS structure for  $n \approx 5-15$ . This idea is certainly consistent with the likelihood of many nearly equivalent energy isomers of the OFS structure. Alternatively, some homogeneous broadening may occur from the direct pumping of vibrational excitation into roughly normal modes of the R's, which then flows into a local model leading to the "boiling off" (dissociation) of an R and the concomitant lifetime broadening.

The remaining characteristics (3.c and d) of the broad line structure and the approach to the matrix limit can be viewed as the evolution and modification of the OFS picture. As would be expected, the details of this evolution differ from inert gas to inert gas as the properties of their solid phases are obviously different.

In the case of He (see Fig. 6), the highest complexes favor a second distinct broad peak whose maximum is red shifted roughly  $50 \text{ cm}^{-1}$  from the first broad peak. We believe this peak can be attributed to a two-sided structure, the COFS. This peak is clearly far to the blue of the origin of the LIF spectrum of the CFS structure of  $\text{C}_6\text{F}_6^+ \cdot \text{He}_2$ . At the highest pressures, this latter structure shows some broadening probably indicating slight additional clustering of the symmetrical  $\text{C}_6\text{F}_6^+ \cdot \text{He}_2$  structure. Nonetheless, the limiting cluster configuration appears to follow from the COFS line, which as might be expected from this picture is somewhat sharper than its single-sided OFS counterpart to the blue of the  $0_0^0$  band of  $\text{C}_6\text{F}_6^+$ .

The higher Ne cluster spectra are quite complex. However, we see the clear emergence at the highest pressures of a relatively sharp feature at the matrix limit, which is again sharper and red shifted from the first

broad LIF feature. The latter we attribute to the OFS while the former is the final COFS structure. A fairly strong broad line at the low frequency end of the spectrum, Fig. 8, we attribute to larger clusters built around a symmetrical CFS, which, however, again appears to be a closed route as far as evolution to the matrix is concerned. A final weak broad peak between the OFS and COFS structure we attribute to some other mixed open and closed faced isomeric cluster, which again does not lead to the dominant matrix configuration.

For Ar, the situation is relatively simple. The OFS transition which initially has a maximum with a red shift of  $\sim 110\text{ cm}^{-1}$  (compared to  $785\text{ cm}^{-1}$  for the CFS  $\text{C}_6\text{F}_6^+ \cdot \text{Ar}_2$ ) gradually shifts further to the red as the cluster size grows. It has clearly reached its matrix limit (Fig. 9) of  $\sim 250\text{ cm}^{-1}$  red shift at the highest cluster sizes observed. In contrast to He and Ne, there is no distinct transition between OFS and COFS structures. We suspect that the larger size of Ar causes the cluster to smoothly grow around the ring rather than having two well defined halves. In the larger cluster domain, there is a second broad line further red shifted. Again, we attribute this to another isomeric structure closed to final evolution to the matrix. In this case, it likely consists of one Ar occupying a primary position on the  $\text{C}_6$  axis on one side of the ring, i.e. a 1R-OFS structure. All of the assignments for the broad LIF lines are indicated in Table II.

#### D. Cluster Growth

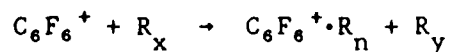
Perhaps the most surprising thing about the clusters is the importance of the OFS structure both for explaining a number of the dominant broad lines in the LIF spectrum and the final closing of these structures leading to the eventual matrix configuration. These structures are not the

intuitively obvious species, especially considering the existence of the symmetric species with the R's on the ion's six-fold axis. The question naturally arises as to why the OFS structures are so prominent in the jet.

It is our belief that at least two cluster growth mechanisms favor the OFS structures. The relative importance of these mechanisms will depend upon the inert gas R. It is important to remember that the growth of these ionic clusters is inherently difficult in the expansion. In producing a neutral van der Waals cluster, the cluster molecule is co-expanded through the nozzle with the inert gas. In the first few nozzle diameters, many-body collisions are probable and the cluster grows.

For the ionic clusters, we have previously argued that the cluster grows predominantly from an isolated ion,<sup>34</sup> (as opposed to ionizing a neutral  $C_6F_6^+ \cdot R_n$  cluster which becomes an ionic cluster  $C_6F_6^+ \cdot R_{n-x}$  where  $x < n$ ). The isolated ions are generally produced at  $\gtrsim 5$  nozzle diameters downstream of the nozzle by the photoionization laser. In this region, there are few multi-body collisions so cluster growth is difficult even for an ion with its long-range attractive potential.

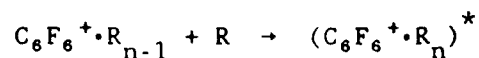
For these reasons, any cluster growth mechanism that effectively proceeds by "two-body" collisions will be highly favored. The most obvious mechanism is growth from preformed  $R_x$  clusters, i.e.



where  $n + y = x$ . Such a reaction would most simply deposit the  $n$  R's on one face of the ring, naturally leading to the OFS structure. This mechanism has parallels with the "pick-up" mechanism espoused by the Scoles group<sup>35</sup> which produces a guest molecule on the surface of a cluster rather than embedded in it. Such a mechanism is likely to be particularly important for a heavier inert gas like Ar which would readily form  $R_n$

clusters during the expansion. In the case of He, however, the presence of significant numbers of  $\text{He}_n$  clusters is questionable.

The second mechanism involves forming a metastable cluster via a true two-body collision, i.e.



The metastable cluster,  $(\text{C}_6\text{F}_6^+ \cdot \text{R}_n)^*$ , can then be stabilized by another two body collision or may simply have a lifetime longer than the timescale of the experiment. The first few adducts are clearly the rate limiting steps in any cluster growth. Suppose  $\text{C}_6\text{F}_6^+ \cdot \text{R}_{n-1}$  is an OFC with small  $n$ . The probability that the additional atom  $\text{R}$  hits the side with inert gas atoms present is at least equal to its hitting the "bare" side. However, the probability of its "sticking" to the sandwich side is much greater. As we saw earlier, the sandwich side, containing  $(n-1)$  inert gas atoms, may be relatively fluid with many low frequency modes to soak up the excess translational energy yielding  $(\text{C}_6\text{F}_6^+ \cdot \text{R}_n)^*$ . Once the complex is formed, a subsequent collision with another  $\text{R}$  is likely to be cooling rather than dissociative, due to the abundance of energy levels and the relatively deep well created by at least a partial ion- $\text{R}$  bond. On the other hand, should  $\text{R}$  strike the bare side of the ion, there is very little probability of accommodating the excess translational energy in the high frequency modes of the ion or transmitting it to the far side of the ring where the  $\text{R}_{n-1}$  cluster has low frequency modes available. Thus one reaches the conclusion that while an additional atom is roughly equally likely to hit the bare or complexed side of the ion, an atom hitting the complexed side has a much higher probability of sticking, thereby favoring the growth of OFS structures compared to CFS ones.

## REFERENCES

1. A. W. Castleman and R. G. Keesee, *Chem. Rev.* **86**, 589 (1986).
2. T. D. Mark and A. W. Castleman, *Adv. At. Mol. Phys.* **20**, 65 (1985).
3. D. Smith and N. G. Adams, *Top. Cur. Chem.* **89**, 1 (1980).
4. R. J. Bowser and F. J. Weinberg, *Nature* **249**, 339 (1974).
5. H. A. Schwartz, *J. Chem. Phys.* **67**, 5525 (1977) and **72**, 284 (1980).
6. M. Okumura, L. I. Yeh, and Y. T. Lee, *J. Chem. Phys.* **88**, 79 (1988) and M. Okumura, L. I. Yeh, J. D. Myers, and T. Y. Lee, *J. Chem. Phys.* **85**, 2328 (1986).
7. J. M. Price, M. W. Crofton, and Y. T. Lee, *J. Chem. Phys.* **91**, 2749 (1989).
8. L. F. DiMauro, M. Heaven, and T. A. Miller, *Chem. Phys. Lett.* **104**, 526 (1984).
9. N. E. Levinger, D. Ray, M. L. Alexander, and W. C. Lineberger, *J. Chem. Phys.* **89**, 5654 (1988).
10. W. L. Liu and J. M. Lisy, *J. Chem. Phys.* **89**, 605 (1988).
11. W. C. Wiley and I. H. McLaren, *Rev. Sci. Instrum.* **26**, 1150 (1955).
12. J. R. Heath, S. C. O'Brien, Q. Zhong, Y. Liu, R. F. Curl, H. W. Kroto, F. K. Tittle, and R. E. Smalley, *J. Am. Chem. Soc.* **107**, 7779 (1985); H. W. Kroto, J. R. Heath, S. C. O'Brien, F. R. Curl, and R. E. Smalley, *Nature* **318**, 162 (1985).
13. M. E. Geusic, T. J. McIlrath, M. F. Jarrold, L. A. Bloomfield, R. R. Freeman, and W. L. Brown, *J. Chem. Phys.* **84**, 2421 (1986).
14. P. A. Freedman, *Can. J. Phys.* **55**, 1387 (1977).
15. Y. Achiba, K. Sato, and K. H. Kimura, *J. Chem. Phys.* **82**, 3959 (1985).
16. J. C. Miller, *Anal. Chem.* **58**, 1702 (1986).
17. P. M. Johnson, M. R. Berman, and D. Zakheim, *J. Chem. Phys.* **62**, 2500 (1975).
18. D. Zakheim and P. M. Johnson, *J. Chem. Phys.* **68**, 3644 (1978).
19. H. Zacharias, R. Schmiedl, and K. H. Welge, *Appl. Phys.* **21**, 127 (1980).
20. R. E. Demaray, C. Otis, K. Aron, and P. Johnson, *J. Chem. Phys.* **72**, 5772 (1980).



21. T. Ebata, N. Mikami, and M. Ito, *J. Chem. Phys.* **78**, 1132 (1983).
22. J. C. Miller and R. N. Compton, *J. Chem. Phys.* **84**, 675 (1986).
23. J. C. Miller and W. C. Cheng, *J. Phys. Chem.* **89**, 1647 (1985).
24. R. A. Kennedy and T. A. Miller, *J. Chem. Phys.* **85**, 2326 (1986).
25. C.-Y. Kung, T. A. Miller, and R. A. Kennedy, *Phil. Trans. Roy. Soc. (Lond) A*, **324**, 223 (1988).
26. R. A. Kennedy, T. A. Miller, and B. Scharf, *J. Chem. Phys.* **85**, 1336 (1986).
27. J. Jortner, U. Even, S. Leutwyler, and Z. Berkovitch-Yellin, *J. Chem. Phys.* **78**, 2606 (1983).
28. J. W. Cooley, *Math. Comput.* **15**, 363 (1961).
29. A. Almenningen, O. Bastiansen, R. Seip, and H. M. Seip, *Acta Chem. Scand.* **18**, 2115 (1964).
30. T. M. Miller and B. Bederson, *Adv. Atom. Molec. Phys.* **13**, 1 (1977).
31. M. H. Ondrechen, Z. Berkovitch-Yellin, and J. Jortner, *J. Am. Chem. Soc.* **103**, 6586 (1981).
32. U. Even, N. Ben-Horin, and J. Jortner, *Phys. Rev. Lett.* **62**, 140 (1989).
33. M. Y. Hahn and R. Whetten, *Phys. Rev. Lett.* **61**, 1190 (1988).
34. R. A. Kennedy, C.-Y. Kung, and T. A. Miller, in *Ions and Ionic Cluster Spectroscopy and Structure* edited by J. P. Maier (Elsevier, 1989), p. 213.
35. T. E. Gough, M. Mengel, P. A. Rountree, and G. Scoles, *J. Chem. Phys.* **83**, 4958 (1985); D. J. LeVandier, M. Mengel, R. Pursel, J. McCombie, and G. Scoles, *Z. Physik D* **10**, 337 (1988).

TABLE I

Relative Signal Strengths of the Broad LIF Peaks to that of the Sharp  $0_0^0$  Band of Uncomplexed  $C_6F_6^+$  and the Corresponding Ratio of  $C_6F_6^+ \cdot He_n$  ( $n \geq 2$ ) Cluster Peak Intensities to that of  $C_6F_6^+$  from the TOF Spectrum.

<u>Trial</u> <sup>a</sup>	LIF $\int \text{Broad} / 0_0^0 C_6F_6^+$	TOF $\sum C_6F_6^+ \cdot He_n / C_6F_6^+$
1	0.6	0.01
2	1.3	0.04
3	2.7	0.07
4	4.1	0.13
5	10.0	0.34

---

<sup>a</sup>The trials correspond to the traces in Fig. 7 with the bottom being number one and increasing upwards in order.

TABLE II

Characteristics of LIF Spectra of Clusters,  $C_6F_6^+ \cdot R_n$   
and Proposed Structural Assignments.

He			
Peak	Type	Shift <sup>a</sup>	Structure
1	Sharp	-38	$C_6F_6^+ \cdot He$
2	Sharp	-81	CFS $C_6F_6^+ \cdot He_2$
3	Broad	+12	OFS $C_6F_6^+ \cdot He_n$
4	Broad	-50	COFS $C_6F_6^+ \cdot He_n$
Ne			
1	Sharp	-56	$C_6F_6^+ \cdot Ne$
2	Broad	+18	OFS $C_6F_6^+ \cdot Ne_n$
3	Broad	-56	COFS $C_6F_6^+ \cdot Ne_n$
4	Broad	-16	1R-OFS $C_6F_6^+ \cdot Ne_n$
5	Broad	-102	CFS $C_6F_6^+ \cdot Ne_n$
6	Matrix	-58	-
Ar			
1	Sharp	-420	$C_6F_6^+ \cdot Ar$
2	Sharp	-785	CFS $C_6F_6^+ \cdot Ar_2$
3	Broad	-255	COFS $C_6F_6^+ \cdot Ar_n$
4	Broad	-425	1R-OFS $C_6F_6^+ \cdot Ar_n$
5	Matrix	-255	-

<sup>a</sup>The shifts are given in  $cm^{-1}$  relative to the  $0_0^0$  band of  $C_6F_6^+$ . The position refers to the peak of the sharp bands and the maximum of the broad ones.

TABLE III

Comparison of Neutral and Ionic Clusters.

	Red Shifts	
	He	Ar
Benzene	2.4 <sup>a</sup>	21 <sup>c</sup>
s-tetrazine	1.4 <sup>b</sup>	23 <sup>d</sup>
C <sub>6</sub> F <sub>6</sub> <sup>+</sup>	38.0 <sup>e</sup>	420 <sup>e</sup>

<sup>a</sup>S. M. Beck, M. G. Liverman, D. L. Monts, and R. E. Smalley, *J. Chem. Phys.* **70**, 232 (1979).

<sup>b</sup>R. E. Smalley, L. Warton, and D. H. Levy, *J. Chem. Phys.* **69**, 2487 (1978).

<sup>c</sup>J. A. Menapace and E. R. Bernstein, *J. Phys. Chem.* **91**, 2533 (1987).

<sup>d</sup>D. V. Brumbaugh, J. E. Kenny, and D. H. Levy, *J. Chem. Phys.* **78**, 3415 (1983).

<sup>e</sup>This work.

TABLE IV

Results of Theoretical Calculations on the  
Vibrational Energy Levels of  $C_6F_6^+ \cdots He$

Level (s b <sub>1</sub> b <sub>2</sub> )	Zeroth Order Energy/cm <sup>-1</sup>	First Order Energy/cm <sup>-1</sup>	Energy from Diagonalization/cm <sup>-1</sup>	Experiment/cm <sup>-1</sup>
(000)	0.0	0.0	0.0	0.0
(100)	48.5	45.3	47.7	41.5
(020) + (002)	43.6	44.0	33.8	48.4
(040) + (004)	67.0	66.5	57.4	66.4
(200)	77.9	70.8	72.3	75.3

TABLE V

$C_6F_6^+ \cdots Ne$  Experimental Observations  
and Results of Theoretical Calculations

Identification	Shift relative to bare ion origin/cm <sup>-1</sup>	Shift relative to cluster origin/cm <sup>-1</sup>	Theory	Vibrational Energy Level
1	-57.4	0.0	0.0	(000)
2	-20.6	36.8	34.0	(100)
3	-17.4	40.0	26.39	(020)
4	-6.5	50.9	48.79	(040)
			63.42	(200)

# FIGURE CAPTIONS

1. Schematic representation of the apparatus used in the experiments.
2. Mass spectrum of  $(\text{NO})_x^+ \text{Ar}_y$  clusters over the mass range from 25 to 625 amu. Cluster combinations with  $x = 1-4$  and  $y = 0-15$  are clearly observed. In addition, several peaks corresponding to  $(\text{NO})_x^+ \text{Ar}_y \cdot \text{H}_2\text{O}$  are also identified. These are due to a small amount of  $\text{H}_2\text{O}$  impurity in the reservoir gases. Intentional additions of  $\text{H}_2\text{O}$  to the reservoir greatly increased the intensity of these peaks. One caution should be noted with respect to cluster identifications. Within the resolution of our TOF, the masses of clusters  $(\text{NO})_x^+ \text{Ar}_y$  and  $(\text{NO})_{x+4}^+ \text{Ar}_{y-3}$  are identical. In labelling this figure, we have assumed that for all peaks  $x \leq 4$ .
3. Mass spectrum in range of 25-450 amu showing clusters  $(\text{NO})_x^+ \text{Ar}_y$ . The numbers above the peaks give the values of  $x$  and  $y$ , respectively. As has been noted below Fig. 2, within the resolution of our TOF the masses of clusters  $(\text{NO})_{x+4}^+ \text{Ar}_{y-3}$  are identical. The top pair of numbers above each peak in the figure give the minimum value for  $y$  while the pairs of numbers below give other allowable combinations. Based upon a logical extrapolation from abundances in the low  $x$  region where there is no ambiguity, it is likely that the pure NO clusters (top numbers) dominate each peak. In any case, it may be noted that peaks, at worst, are comprised of only even or odd numbers of NO's, so that an ambiguity in exact NO's present cannot effect the odd-even variations discussed in the text.
4. Mass spectrum showing cluster ions,  $(\text{NO})_x^+$ ,  $x = 11-15$ . A clear alternation in intensity between even and odd numbers of NO is observable.

5. LIF Spectrum of  $C_6F_6^+$ .
6. Broad scan of LIF spectrum of  $C_6F_6^+$  and  $C_6F_6^+ \cdot He_n$  clusters. Reservoir pressures,  $P_0$ , marked with a star indicate experiments in which the photoionization laser was displaced towards the nozzle, i.e. to higher He density, than the corresponding unstarred pressures.
7. Five traces showing simultaneous LIF and TOF spectra of  $C_6F_6^+$  and  $C_6F_6^+ \cdot He_n$ . The traces differ in the density of He at the photoionization point,  $D_{exe}$  in nozzle diameter (N.D.), with a constant 160 psig He reservoir pressure. The lowest trace corresponds to  $D_{exe} \approx 15$  while in the upper traces, the laser was displaced by the indicated distance towards the nozzle. All distances are measured in units of the nozzle diameter.
8. Four traces showing simultaneous LIF and TOF spectra of  $C_6F_6^+$  and  $C_6F_6^+ \cdot Ne_n$  for various Ne reservoir pressures. In the LIF spectra, the vibrational progression in  $C_6F_6^+ \cdot Ne$  is indicated as well as the position of the  $0_0^0$  band observed for  $C_6F_6^+$  in a solid Ne matrix.
9. Four traces showing simultaneous LIF and TOF spectra of  $C_6F_6^+$  and  $C_6F_6^+ \cdot Ar_n$  for various percentages of Ar in He held at total reservoir pressures of 200 psig. In the bottom LIF trace, the sharp, but complex, vibrational progressions of  $C_6F_6^+ \cdot Ar_n$  with  $n = 1$  and 2 are indicated, while in the top trace the position of the  $0_0^0$  band of  $C_6F_6^+$  in a solid Ar matrix is indicated.
10. Traces showing the effect of variation of temperature,  $T_r$ , of the  $C_6F_6$  vessel and hence its partial pressure in the expansion. The total pressure of the Ar/He reservoir is 200 psig.



11. Side-on view of a space-filling model of the  $C_6F_6^+$  cation complexed by two Ne's lying on the  $C_6$  axis symmetrically above and below the plane of the hexagon. This is an example of a closed-faced sandwich (CFS) structure.
12. Fluorescence excitation spectra of  $C_6F_6^+ \cdot He$  and  $C_6F_6^+ \cdot Ne$  associated with the origin transition of  $C_6F_6^+$ .
13. Contour plot of the  $V(x,0,z)$  cut of the potential for  $C_6F_6^+ \cdot He$  described in the text. The minimum is located 2.43 Å above the plane of the  $C_6F_6^+$  ring. Contours are plotted every 10  $cm^{-1}$ .
14. Side-on view of a space filling model of the  $C_6F_6$  cation complexed by four Ne atoms. Two of the Ne atoms occupy the symmetrical  $C_6$  axis sites depicted in Fig. 7, while the other two are obligated to occupy "secondary" sites. This is an example of a closed-faced sandwich (CFS) structure.
15. Top view of a space filling model of the  $C_6F_6$  cation complexed by four Ne atoms. In contrast to Fig. 7, all four atoms occupy roughly equivalent sites, but none are on the  $C_6$  axis. This is an example of an open-faced sandwich (OFS) structure.

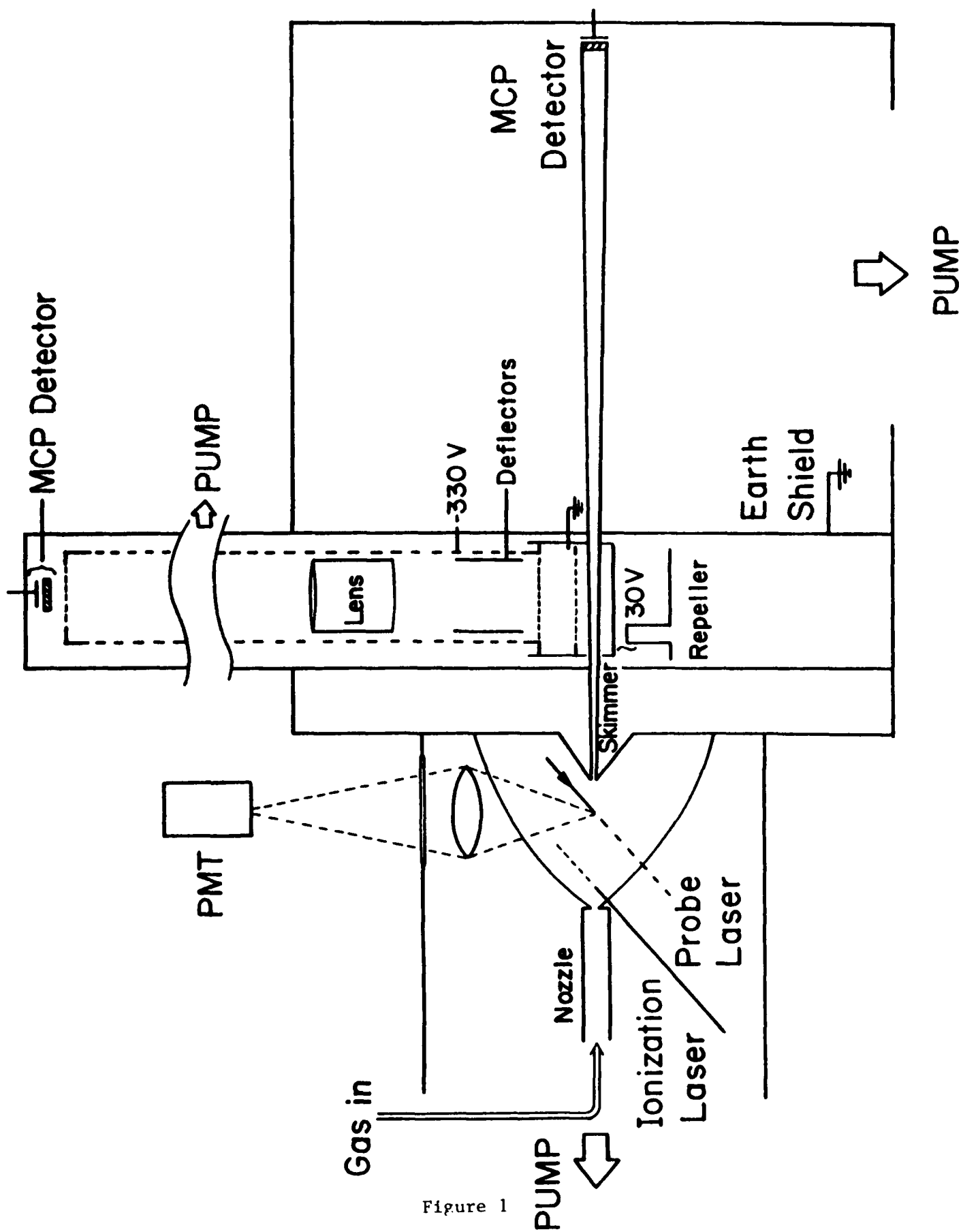


Figure 1



$(\text{NO})_x^+ \text{Ar}_y$   
 2.4% NO  
 200 psi Ar

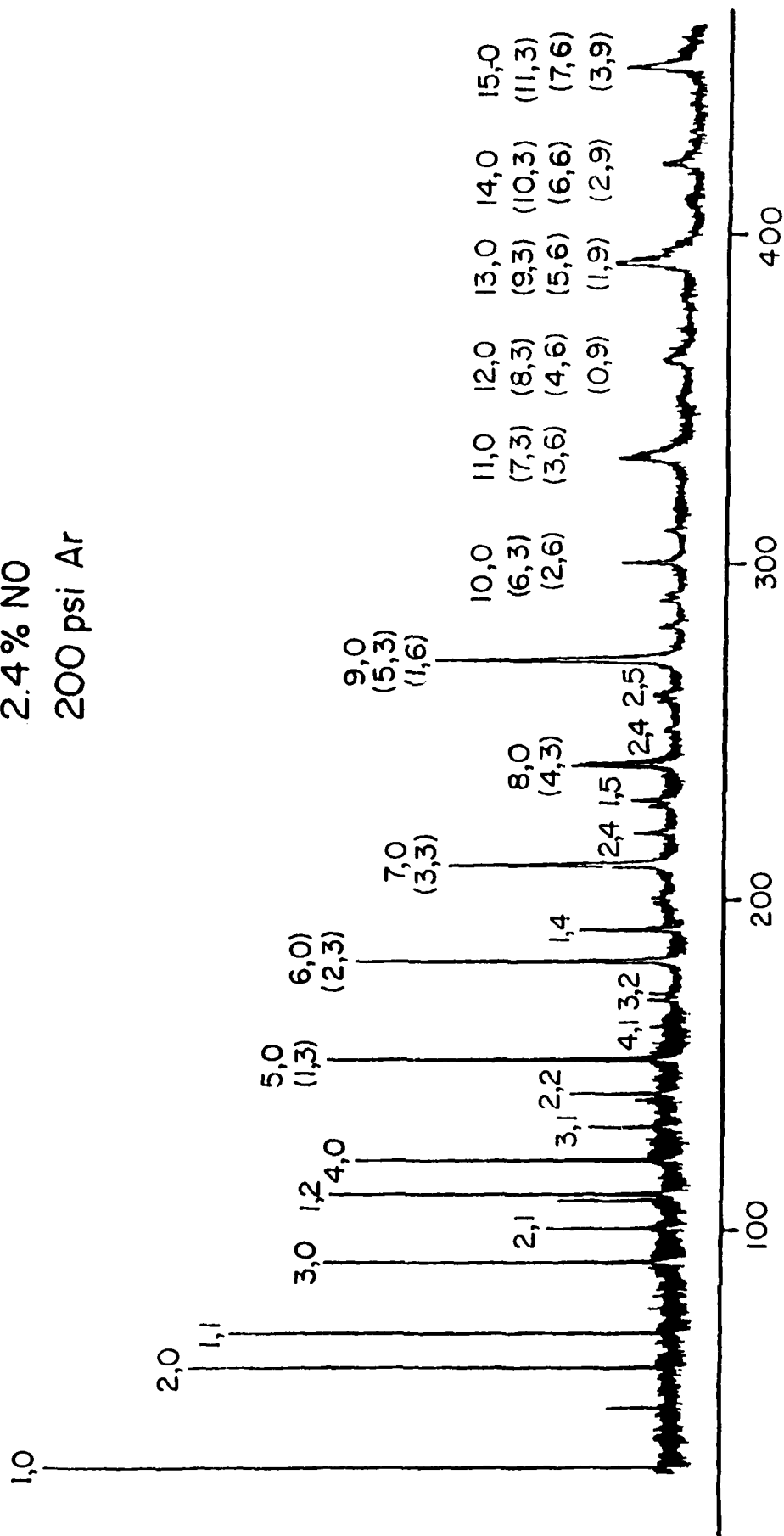


Figure 3

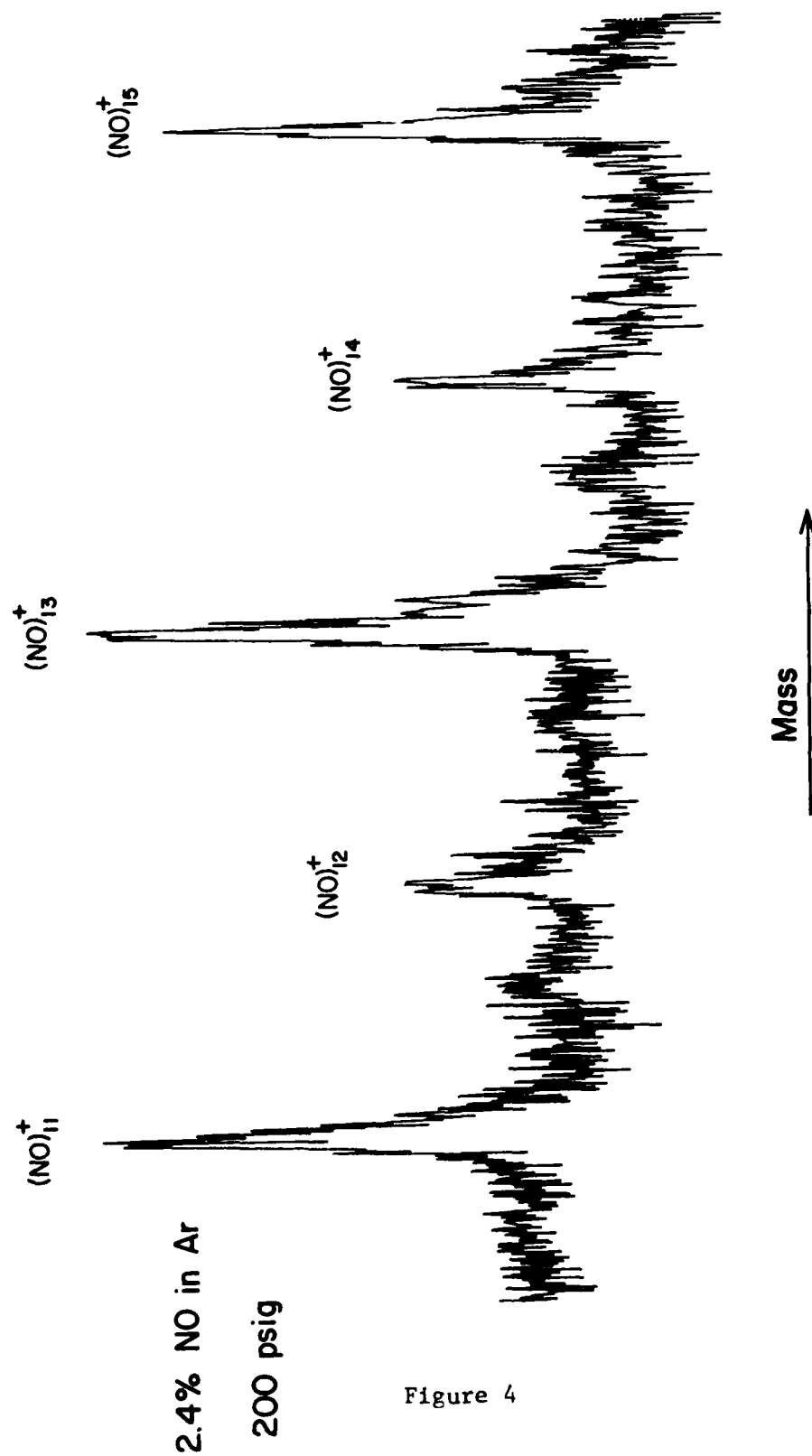


Figure 4

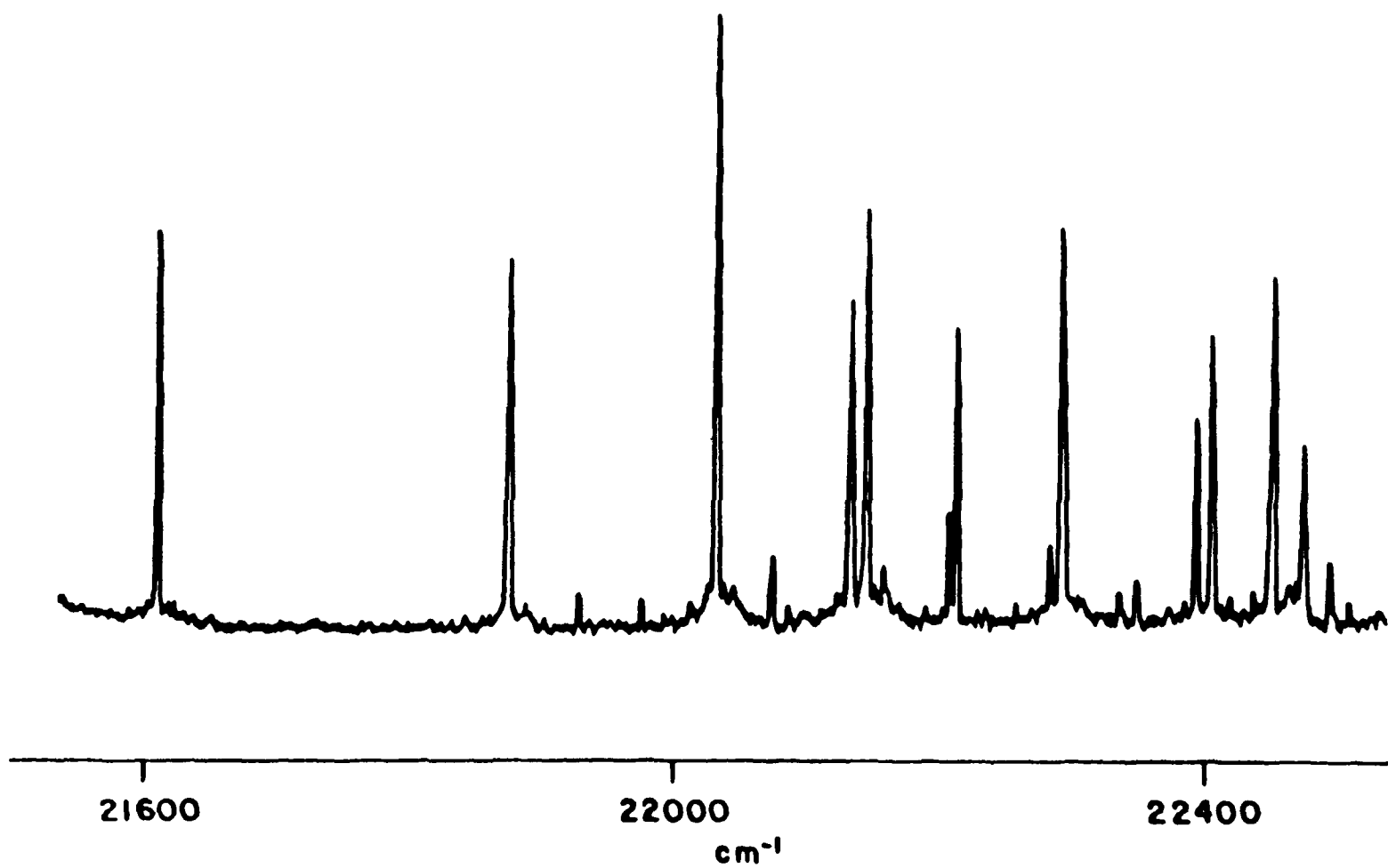


Figure 5

# LIF of $C_6F_6^+$ in He

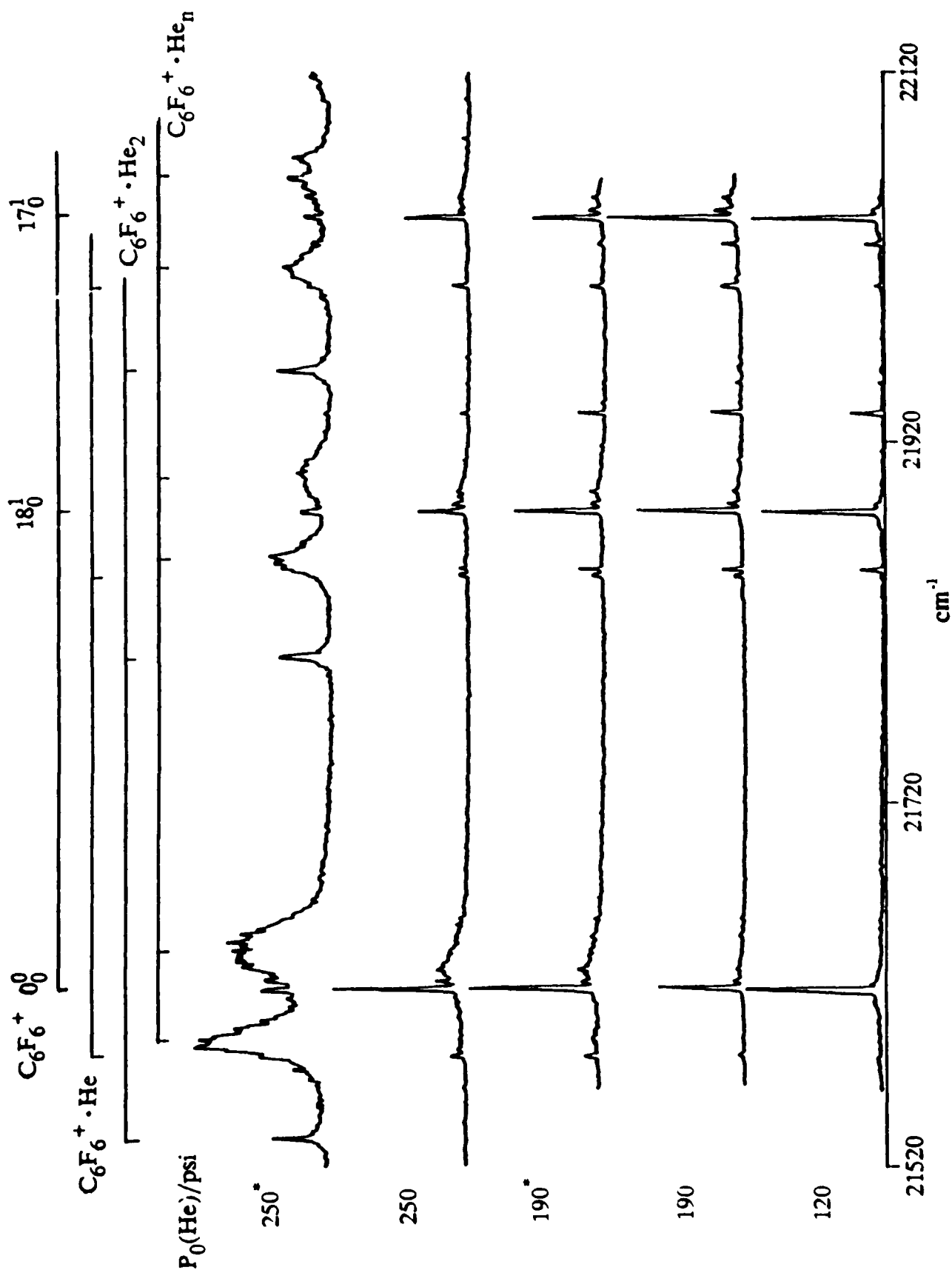


Figure 6

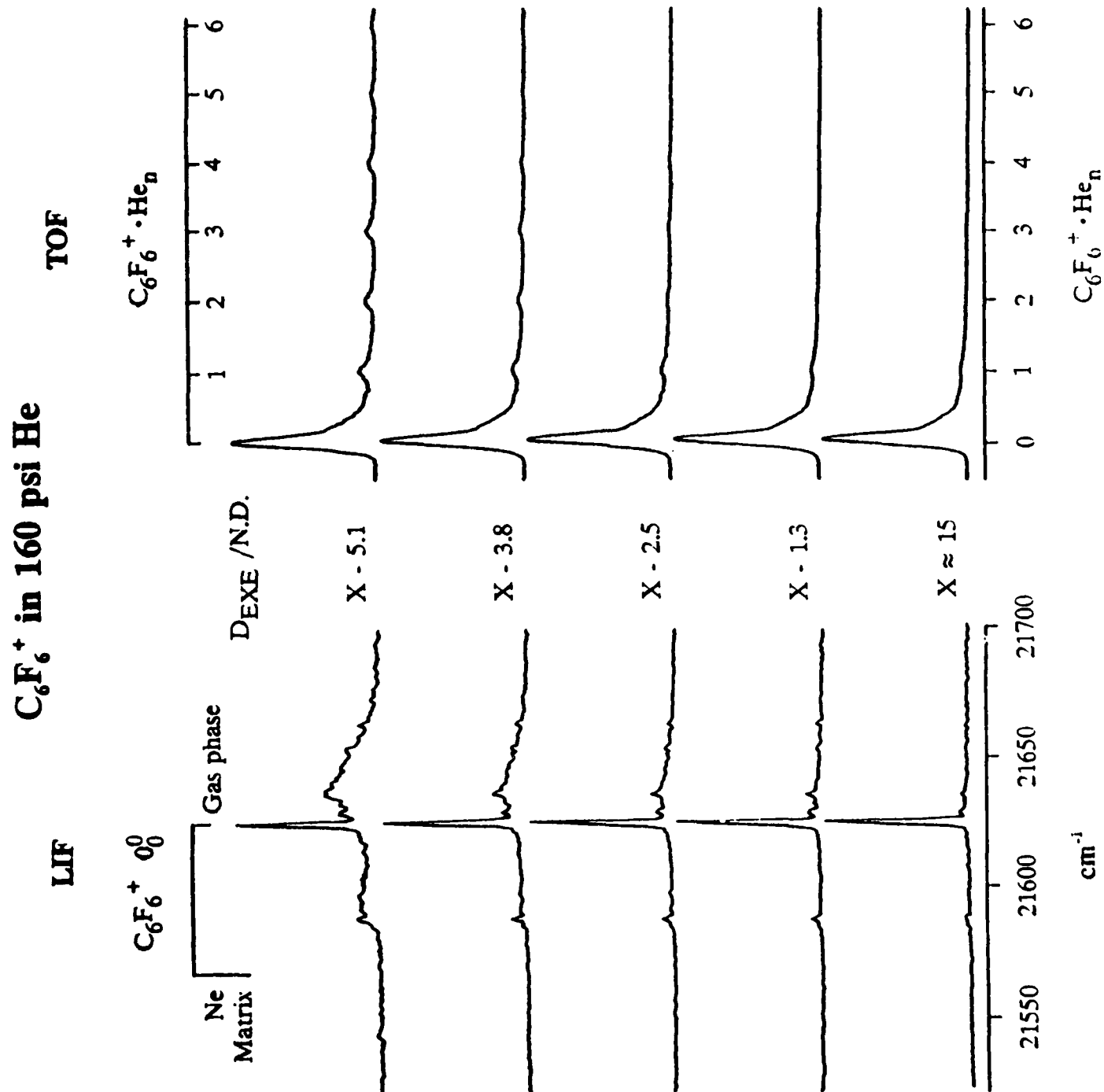


Figure 7



# $C_6F_6^+$ in Ne

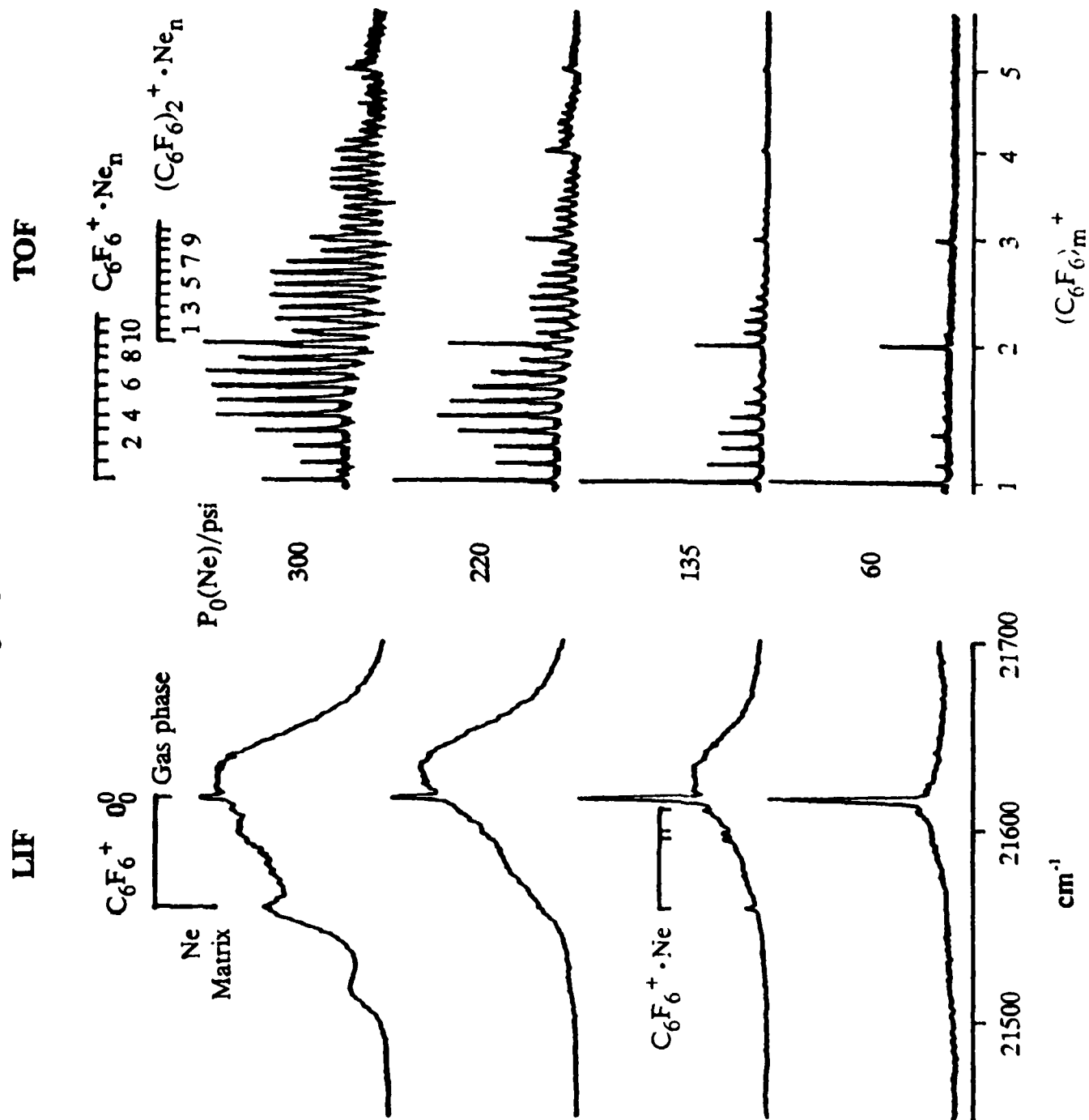


Figure 8

# $C_6F_6^+$ in Ar/He

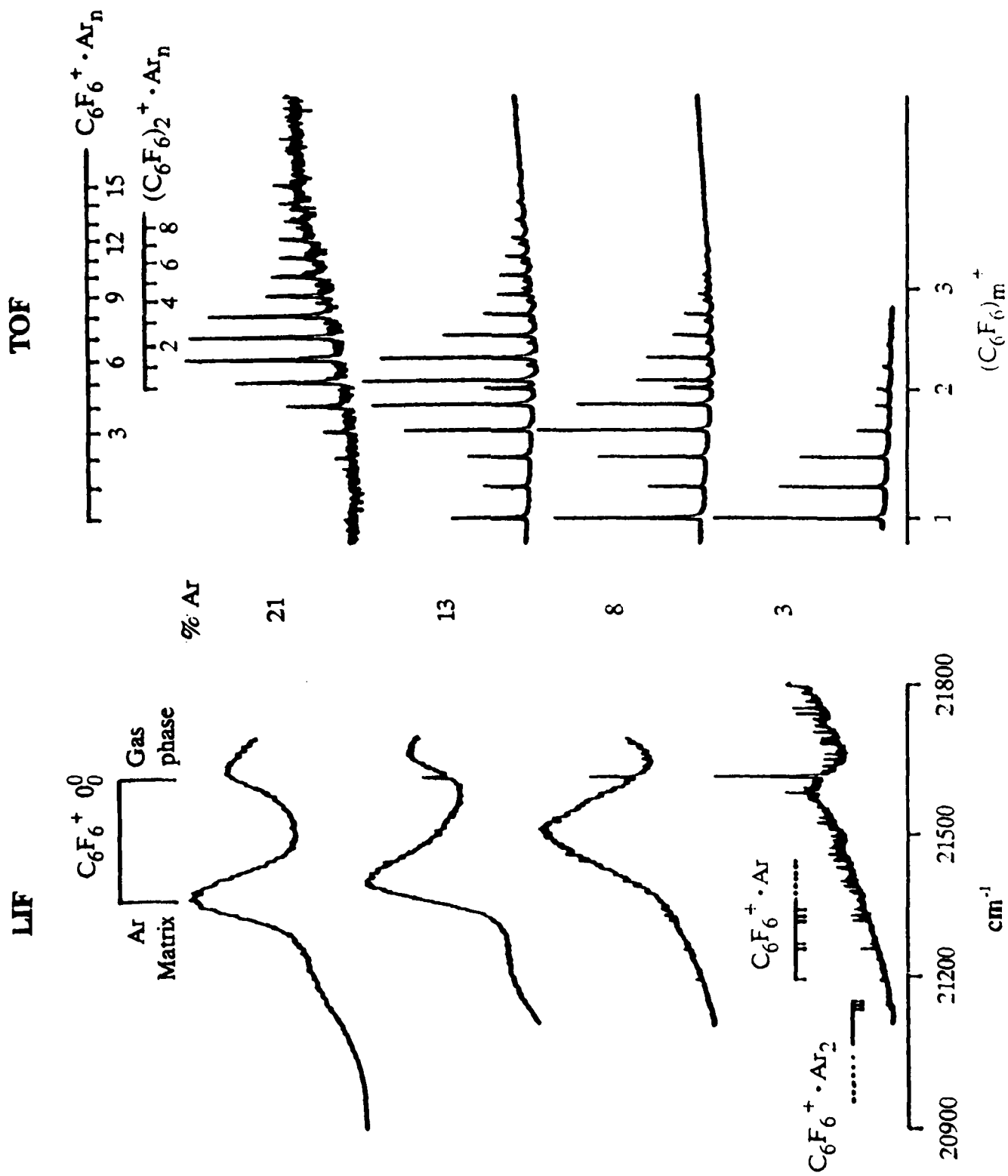


Figure 9

# $C_6F_6^+$ in 8% Ar/He

LIF

TOF

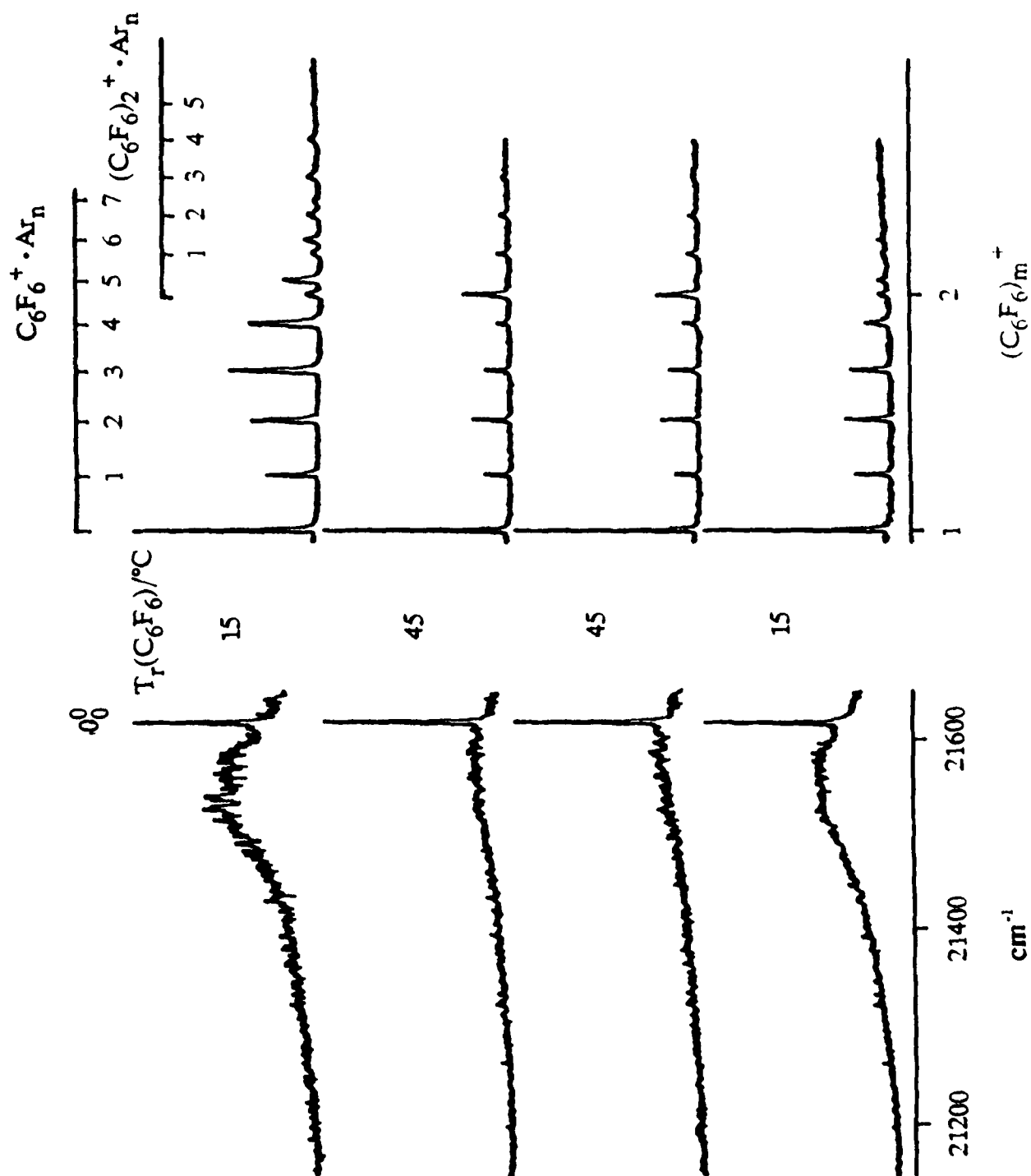


Figure 10

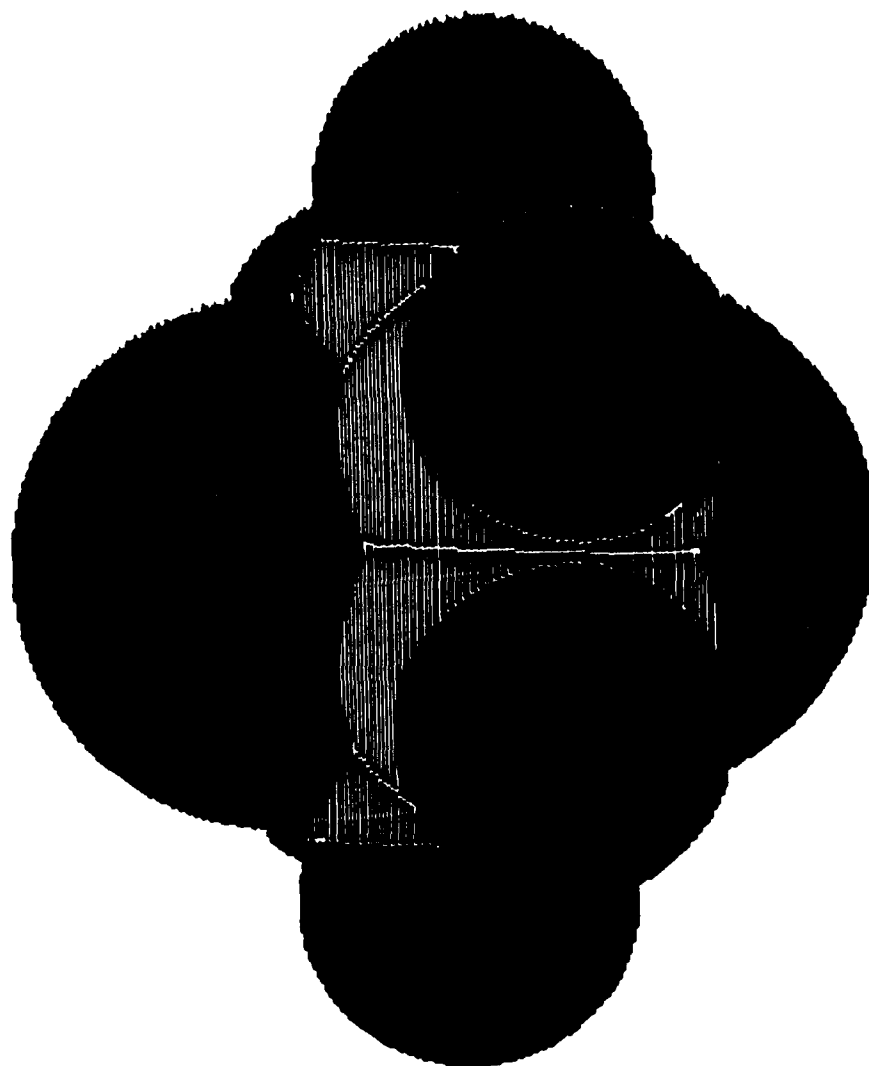


Figure 11

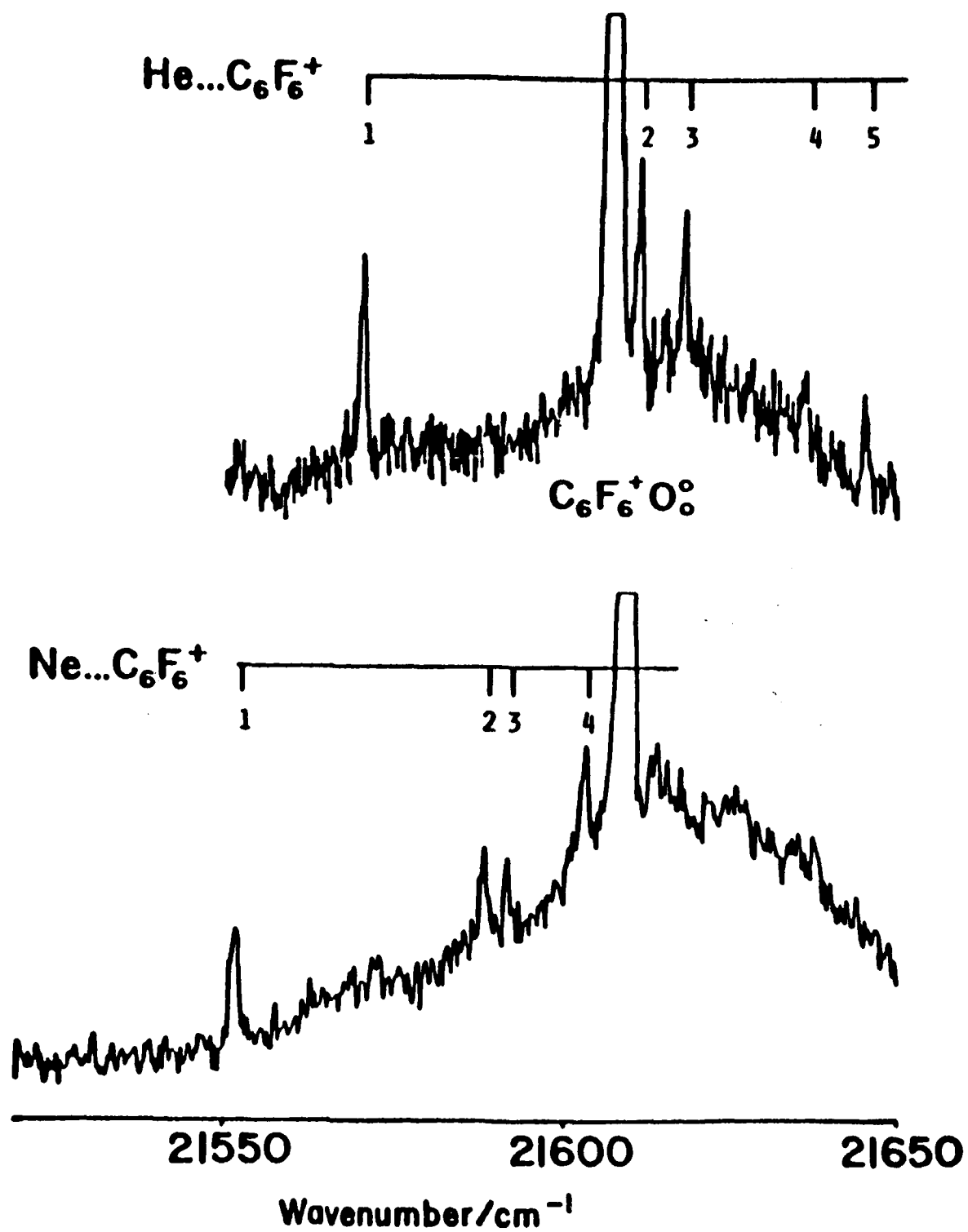


Figure 12

# $\text{C}_6\text{F}_6^+-\text{He}$ : Vertical Section of the potential

$V/\text{cm}^{-1}$

-10

-30

-50

-70

-90

-110

-130

-130

+100

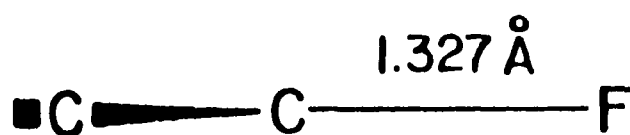
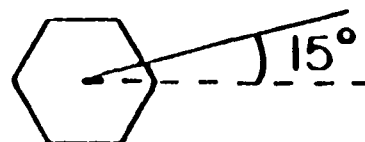


Figure 13

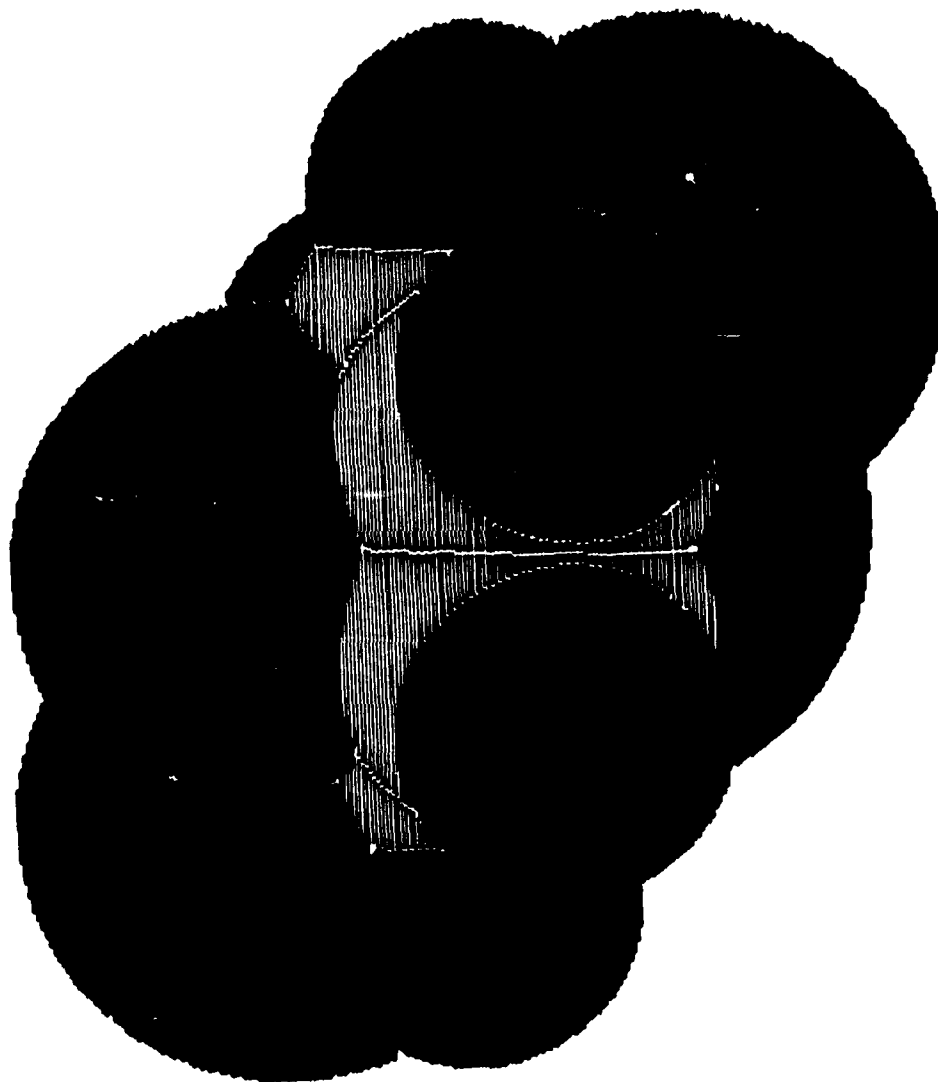


Figure 14

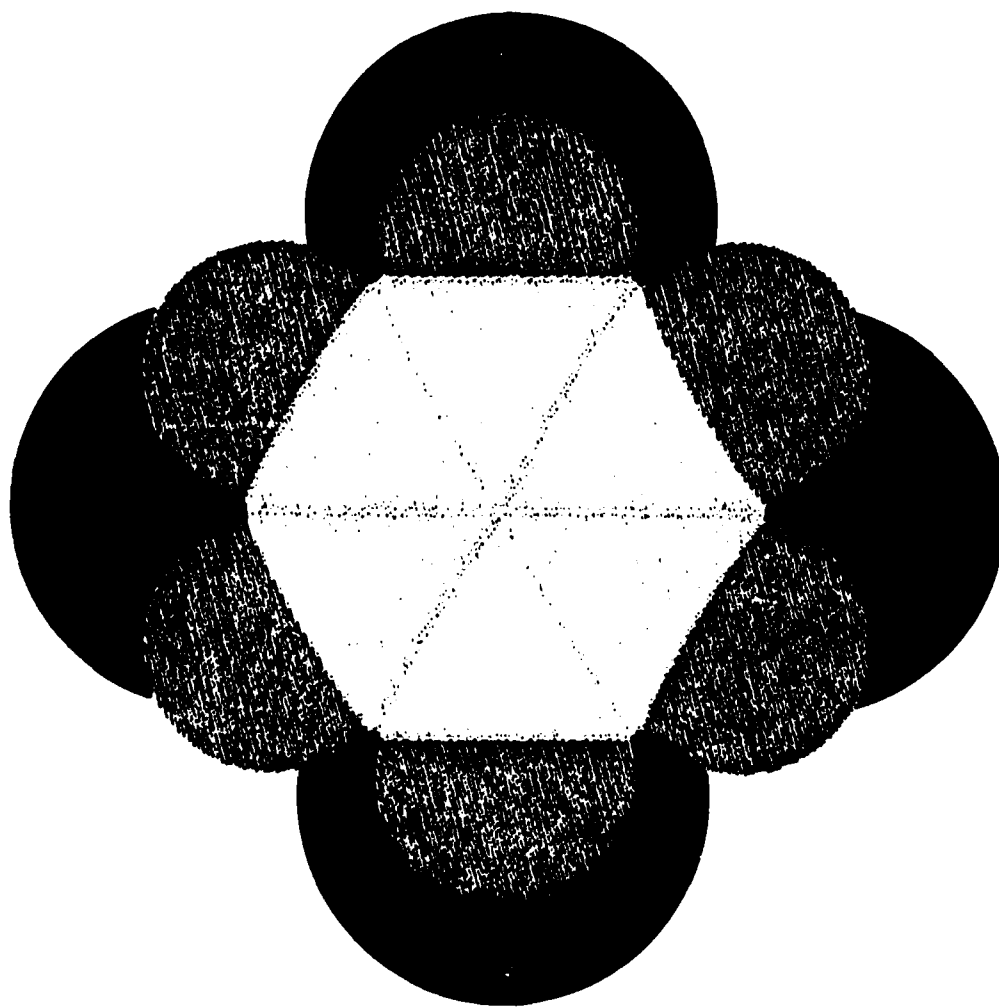


Figure 15